Journal of Quantitative Spectroscopy & Radiative Transfer 255 (2020) 107217

Contents lists available at ScienceDirect

Journal of Quantitative Spectroscopy & Radiative Transfer

journal homepage: www.elsevier.com/locate/jqsrt

Absorption coefficient (ABSCO) tables for the Orbiting Carbon Observatories: Version 5.1

Vivienne H. Payne[a,*], Brian J. Drouin[a], Fabiano Oyafuso[a], Le Kuai[a], Brendan M. Fisher[a], Keeyoon Sung[a], Deacon Nemchick[a], Timothy J. Crawford[a], Mike Smyth[a], David Crisp[a], Erin Adkins[b], Joseph T. Hodges[b], David A. Long[b], Eli J. Mlawer[c], Aronne Merrelli[d], Elizabeth Lunny[e], Christopher W. O'Dell[f]

[a] NASA Jet Propulsion Laboratory, California Institute of Technology, 4800 Oak Grove Drive, Pasadena, CA 91109 United States
[b] Material Measurement Laboratory, National Institute of Standards and Technology, 100 Bureau Drive, Gaithersburg, MD 20899, USA
[c] Atmospheric and Environmental Research, Lexington, MA, USA
[d] Space Science and Engineering Center, University of Wisconsin - Madison, Madison, WI 53706, USA
[e] California Institute of Technology, 1200 East California Boulevard, Pasadena, CA 91125, USA
[f] Colorado State University, Fort Collins, CO 80523, USA

ARTICLE INFO

Article history:
Received 14 April 2020
Revised 13 July 2020
Accepted 13 July 2020
Available online 6 August 2020

Keywords:
Oxygen
Carbon dioxide
Absorption
Atmosphere
CIA
Line-mixing

ABSTRACT

The accuracy of atmospheric trace gas retrievals depends directly on the accuracy of the molecular absorption model used within the retrieval algorithm. For remote sensing of well-mixed gases, such as carbon dioxide (CO_2), where the atmospheric variability is small compared to the background, the quality of the molecular absorption model is key. Recent updates to oxygen (O_2) absorption coefficients (ABSCO) for the 0.76 µm A-band and the water vapor (H_2O) continuum model within the 1.6 µm and 2.06 µm CO_2 bands used within the Orbiting Carbon Observatory (OCO-2 and OCO-3) algorithm are described here. Updates in the O_2 A-band involve the inclusion of new laboratory measurements within multispectrum fits to improve relative consistency between O_2 line shapes and collision-induced absorption (CIA). The H_2O continuum model has been updated to MT_CKD v3.2, which has benefited from information from a range of laboratory studies relative to the model utilized in the previous ABSCO version. Impacts of these spectroscopy updates have been evaluated against ground-based atmospheric spectra from the Total Carbon Column Observing Network (TCCON) and within the framework of the OCO-2 algorithm, using OCO-2 soundings covering a range of atmospheric and surface conditions. The updated absorption coefficients (ABSCO version 5.1) are found to offer improved fitting residuals and reduced biases in retrieved surface pressure relative to the previous version (ABSCO v5.0) used within B8 and B9 of the OCO-2 retrieval algorithm and have been adopted for the OCO B10 Level 2 algorithm.

1. Introduction

1.1. Spaceborne observations of CO_2 using near-infrared spectral bands

Space-based remote sensing retrievals of carbon dioxide (CO_2) provide opportunities for improved understanding of the global carbon cycle by enabling observation of regions of the globe where ground-based networks do not have coverage.

Current and future satellite missions such as the Greenhouse gases Observing SATellites (GOSAT and GOSAT-2) [19], the NASA Orbiting Carbon Observatory missions (OCO-2 and OCO-3) [8,12], TanSat [54] and GeoCARB [30,35] rely on measurements of the absorption of reflected sunlight by oxygen (O_2) and CO_2. From these measurements, estimates of the column-averaged CO_2 dry air mole fraction, (XCO_2), can be retrieved e.g. O'Dell et al. [31]. The CO_2 concentration fields can then be used within atmospheric inversion frameworks to infer sources and sinks of CO_2. Results of these atmospheric inversions, which are dependent on small differences in large numbers, can be strongly impacted by systematic errors in the retrieval of XCO_2. Regionally-dependent biases are of particular concern, since these could affect the estimates of the sources and sinks [1,5,7,25]. The accuracy of the molecular absorption model used within the retrievals is therefore a key consideration for the accuracy of the retrieved XCO_2 products.

* Corresponding author.
E-mail address: Vivienne.H.Payne@jpl.nasa.gov (V.H. Payne).

https://doi.org/10.1016/j.jqsrt.2020.107217

The OCO missions utilize spectrally resolved measurements in the 0.76 μm O_2 A-band and 1.6 μm and 2.06 μm CO_2 bands. Calculations of molecular absorption at high spectral resolution over a wide bandwidth using line-by-line models are generally too slow for use within operational retrieval algorithms. For the OCO missions, molecular absorption coefficients (ABSCO) are calculated offline for a range of pressures, temperatures and H_2O volume mixing ratios and stored in look-up tables (known as ABSCO tables). Successive versions have refined these tables by incorporating new laboratory results and theoretical models for increasingly accurate absorption coefficients. ABSCO tables are released together with each major build of the OCO Level 2 algorithm. The OCO algorithm has also been applied to GOSAT radiances under the NASA Atmospheric Carbon Observations from Space (ACOS) effort. The ABSCO v5.1 tables described in this work are used within Build 10 of the Level 2 algorithm.

The OCO algorithm utilizes ABSCO tables for CO_2, O_2 and H_2O. Tables for CO_2 and O_2 are based on multispectrum fits to laboratory spectra taken at multiple temperatures and pressures. (See [3,9,11] for additional discussion of the multispectrum fitting approach). Further details on the inputs to the tables are provided in the sections that follow. Tables are also calculated for methane (CH_4), using the HITRAN 2012 line parameters and a Voigt line shape. However, because the OCO-2 spectral ranges were specifically selected to avoid CH_4 lines, the few methane lines present at the longwave end of the 1.6 μm CO_2 band do not significantly affect the simulations. CO_2 tables have not been updated between ABSCO v5.0 and v5.1. Updates in ABSCO v5.1 are focused on the O_2 A-band and on H_2O continuum absorption in the 1.6 μm and 2.06 μm CO_2 bands.

1.2. Level 2 XCO_2 retrieval algorithm background

Improvements to the spectroscopy have been a key component of the evolution of the OCO/ACOS algorithm over the years. The approach taken by the OCO team has involved (1) acquisition and analysis of laboratory measurements over a range of temperatures and pressures relevant for atmospheric conditions, (2) validation of resulting ABSCO tables using atmospheric measurements and (3) evaluation of the impacts of any changes on satellite retrievals using a given build of the Level 2 algorithm. The goal is to push the ABSCO tables to contain the best possible heuristic and reductive physical models in order to reduce or eliminate regional biases in the OCO XCO_2 products.

Laboratory measurements can provide the highest spectral resolution and well-characterized temperature, pressure, path length and gas mixtures for individual spectra. Ground-based atmospheric spectra provide validation of the resulting ABSCO tables, for the full atmospheric path, with certain constraints on the atmospheric conditions. Validation of previous versions of ABSCO tables using ground-based atmospheric measurements are described in more detail in [11,33,47]. The ground-based validation described in both this manuscript and previous work relies on single-band retrievals from spectra taken at the Total Column Carbon Observing Network (TCCON) Lamont site [53]. Atmospheric conditions above this site are well-characterized by a range of complementary measurements. The TCCON spectra are direct solar measurements, which are less sensitive to aerosol impacts than the reflected solar measurements from the satellite. Single band retrievals are chosen for the purposes of ABSCO validation to keep the interpretation of results simple.

Evaluation of the impacts of spectroscopic updates on the OCO retrievals involves some extra complexity. The OCO algorithm does a joint retrieval of a number of different parameters using all three bands. In addition, retrievals from satellite measurements of reflected solar radiance require consideration of the representation of surface parameters and aerosol influence. This all makes it important to test spectroscopic updates within a given L2 algorithm to evaluate impacts on satellite retrievals. Soundings taken in glint mode over ocean/water surfaces, with low aerosol optical depth, are the simplest case for evaluation of ABSCO impacts. For soundings over land, the impacts of spectroscopic updates will interact with multiple other sources of systematic error in the retrievals.

To mitigate biases and improve algorithm convergence issues, residuals from each spectral band are aggregated from global data sets and used to develop empirical orthogonal functions (EOFs) that may be subtracted from the data prior to analysis from the retrieval algorithm, such that the persistent residuals would tend to not pull the solution away from the (assumed) unbiased conditions. If the spectroscopic tables, instrument function, and atmospheric *a priori* information were all ideal, these EOFs would be within the measurement noise. The OCO-2 instrument produces spectra for eight spatial footprints. As documented in O'Dell et al. [32], the first EOFs for each of the eight footprints are very similar. In addition, the first EOFs for OCO-2 and GOSAT are very similar for each band, indicating that forward model errors rather than instrument-specific effects are dominant. The evaluation of ABSCO tables/spectroscopy updates within the L2 algorithm uses a configuration where EOFs are not applied. New EOFs are calculated for each algorithm build.

The EOFs can mitigate, but do not eliminate, impacts of spectroscopic errors. The need for further improvements to spectroscopic input for the OCO/ACOS algorithm is highlighted in O'Dell et al. [32], who describe the B8 version of the OCO/ACOS Level 2 algorithm, outstanding issues with the B8 XCO_2 retrieval product and some explanation of why remaining uncertainties in the spectroscopic input to the algorithm may be the underlying explanation for some of these issues. Updates to the bias correction that led to B9 are documented in [17]. The update between B8 and B9 did not involve any changes to the spectroscopy.

Updates to spectroscopy/ABSCO tables comprise an important component of the update between Level 2 B9 and B10. Sources of input for the ABSCO v5.0 (used in B8/B9 Level 2) and ABSCO v5.1 (used in B10 Level 2) are summarized in Table 1.

1.3. Oxygen spectroscopy background

In recent decades, the atmospheric O_2 features in the near-infrared/visible region have gained increasing attention due to their versatile applications in atmospheric remote sensing. Within the OCO Level 2 algorithm, the O_2 A-band near 0.76 μm provides a means to characterize the atmospheric path. This band is dominated by monomer line contributions at standard conditions. However, an extra absorption contribution in observed laboratory and atmospheric spectra has been attributed to the presence of collision induced absorption (CIA) associated with transient molecular O_2 pairs or double transitions interacting with one single

Table 1
ABSCO parameters for v5.0 (OCO L2 B8 and B9) and v5.1 (OCO L2 B10).

Band	0.76 μm	1.6 μm	2.06 μm
Spectral range (cm^{-1})	12,950 to 13,190	6120 to 6260	4800 to 4890
ABSCO version	5.0 / 5.1	5.0 / 5.1	5.0 / 5.1
line shape	*a* / *b*	*f* / *f*	*i* / *i*
line mixing	*a* / *b*	*f* / *f*	*i* / *i*
CIA	*a* / *b*	-	*j* / *j*
H_2O broadening	*c* / *c*	*g* / *g*	*g* / *g*
H_2O continuum	*d* / *e*	*d* / *e*	*d* / *e*
H_2O lines	*h* / *h*	*h* / *h*	*h* / *h*

(*a*) Drouin et al. [11]; (*b*) This work; (*c*) Drouin et al. [10]; (*d*) Mlawer et al. [26]; (*e*) MT_CKD v3.2; (*f*) Devi et al. [9]; (*g*) Sung et al. [44]; (*h*) Rothman et al. [39]; (*i*) Benner et al. [3]; (*j*) Thompson et al. [47].

photon. Two major and experimentally challenging features of the CIA are that (1) it exhibits a continuous and slowly varying function of frequency (or wavenumber) with a quadratic pressure (strictly speaking, number-density) dependence; and (2) features are very weak in a conventional laboratory settings. Nevertheless, the O_2 A-band CIA has been studied in many laboratories for more than five decades [6,24,40–43,46]. The theory developed in [50] and [49] enabled the first extraction of the O_2 A-band CIA with the O_2 A-band monomer resonance contribution modelled by a Voigt profile in the presence of line mixing effects. Drouin et al. [11] used a variant of this line-mixing model in combination with a speed-dependent line profile. Theoretical descriptions of the A-band CIA were provided by [15] with attributions of CIA bandshapes to differing collisional-induced absorption mechanisms. Reviews including discussion of this particular CIA can be found in both the recent HITRAN publication [36] as well as in [14]. Due to the common methods of characterizing CIA through determination of 'leftover' non-resonant absorption, new versions of CIA *must* be developed along with any significant changes of the resonant model.

The ABSCO v5.0 tables were constructed using the analysis described in [11]. The ABSCO v5.1 tables were constructed using an updated analysis, described in Section 2, involving new laboratory measurements and re-analysis of atmospheric data sets.

1.4. Water vapor background

H_2O is a strong interferent in the OCO XCO_2 retrievals. (See, for example, Oyafuso et al. [33] for examples of H_2O line features in TCCON residuals in the 1.6 and 2.06 µm CO_2 bands.) For ABSCO v5.0, tables of H_2O absorption were calculated using the Voigt line shape with parameters from the HITRAN 2012 compilation [39] and the MT_CKD v2.6 H_2O continuum model [26,27].

This "custom" version of the MT_CKD was scaled specifically in the OCO-2 spectral bands, based on an analysis of Lamont TCCON FTS spectra. Since then, laboratory measurements and analyses have become available that provide new constraints on the foreign and self broadened H_2O continua in the OCO bands. MT_CKD foreign continuum coefficients at wavenumbers greater than 4000 cm^{-1} were modified based on [2], and [28] measurements. Self continuum coefficients were updated based on a number of new laboratory studies [4,28,36,52]. These changes have been included in the MT_CKD v3.2 continuum. For ABSCO v5.1, tables of H_2O absorption were calculated using the Voigt line shape with parameters from the HITRAN 2012 compilation [39] and the MT_CKD v3.2 H_2O continuum model. Note that line parameters from HITRAN 2016 were also tested within the ABSCO framework. It has been demonstrated using an evaluation based on a range of laboratory and atmospheric spectra that when considering consistency across all spectral regions, the HITRAN 2016 H_2O line list is an improvement over HITRAN 2012 [48]. However, when considering only the OCO spectral regions, we did not find HITRAN 2016 to offer an advantage in terms of improvements to spectral residuals for atmospheric spectra.

The changes to both the self and foreign induced H_2O continua between MT_CKD v2.6 (used in ABSCO v5.0) and MT_CKD v3.2 (used in ABSCO v5.1) were significant. Fig. 1 shows differences between continuum-only absorption cross-sections calculated using these two different versions, within the OCO bands. For the 2.06 µm band, the updated foreign continuum (denoted by "q=0%", where q is water mixing ratio) of MT_CKD 3.2 is enhanced by nearly a factor of two on the shortwave end of the band and by nearly a factor of four on the longwave end with respect to ABSCO v5.0. For the 1.6 µm band, the high water content case ($q = 6\%$), dominated by the self continuum, decreased by nearly an order of magnitude from MT_CKD 3.2 to ABSCO v5.0. In the 0.76 µm band, the moist air case changes very little, but the dry air continuum shows reductions of nearly an order of magnitude.

2. Methodology

Here we describe new laboratory experiments and new analyses for laboratory, field and satellite data utilized in this study. The experimental and field data analyses methods are similar to previous work and are only summarized here, whereas some additional detail is provided on the satellite data analyses.

2.1. Laboratory experiments

2.1.1. Cavity ring-down spectroscopy (CRDS)

The CRDS O_2 A-band analysis for ABSCO v5.0 was based on room temperature laboratory measurements. In experiments utilized for the analysis for ABSCO v5.1, we have investigated the temperature dependence of the O_2 A-band using a cavity ring-down spectroscopy (CRDS) technique, with a cell developed at the National Institute of Standards and Technology (NIST) initially for studying the temperature dependence of CO_2 line shapes in the 1.6 µm region.

The pressure and temperature dependence of O_2 A-band line shapes were measured with the CRDS over the range 10 Torr (1.3 kPa) to 1000 Torr (133 kPa), and 237 K to 296 K. The low-pressure measurements primarily constrained line position and intensity. The high-pressure measurements guided the refinement of broadening, shift and mixing parameters in concert with determination of CIA. Sample gases included ^{16}O-enriched O_2 in synthetic air. The line-cores in the CRDS spectra are optically thick under the high-pressure conditions (see Fig. 2), so we measured dilute amounts of O_2 in the same bath gas to reduce the optical thickness of the samples so that gap-free spectra could be acquired throughout the line cores. This new dataset augments legacy CRDS data [11,22,23,37] in the current analysis. Further detail on these measurements, including information on the full set of experimental conditions is provided in the supplemental information, along with the data conditions for Fourier Transform Spectrometer (FTS) measurements also utilized in the ABSCO v5.1 analysis.

2.1.2. Laboratory FTS spectra

In addition to FTS spectra recorded and reported in Drouin et al. [11], a high-pressure pure O_2 spectrum was obtained at room temperature using a 1 m long straight-pass stainless steel cell. The FTS instrumental set-up, and subsequent experiments performed after this analysis, are described in detail in Sung et al. [45]. A summary is also provided in the supplement. This additional high pressure FTS spectrum was included in the analysis with the goal of providing additional constraints on line mixing and CIA in the ABSCO v5.1 analysis.

2.1.3. Analysis and evaluation using ground-based TCCON spectra

The method developed for extraction of O_2 A-band CIA from atmospheric measurements using TCCON spectra and shortwave irradiances from the Normal Incidence Multifilter Radiometer (NIMFR) at the Southern Great Plains (SGP) site of the DoE Atmospheric Radiation Measurement (ARM) in Lamont, Oklahoma [11] is further utilized in this effort. In consultation with the TCCON team, ten sample days from time periods when the TCCON spectrometer was deemed to have been operating well were chosen. The dates were selected with the goal of spanning a good range of the atmospheric temperatures and column water vapor conditions encountered at Lamont. The set of ten days includes six from winter/spring (20120102, 20120106, 20120110, 20120206, 20120226 and 20120329) and four from summer (20120618, 20120623,

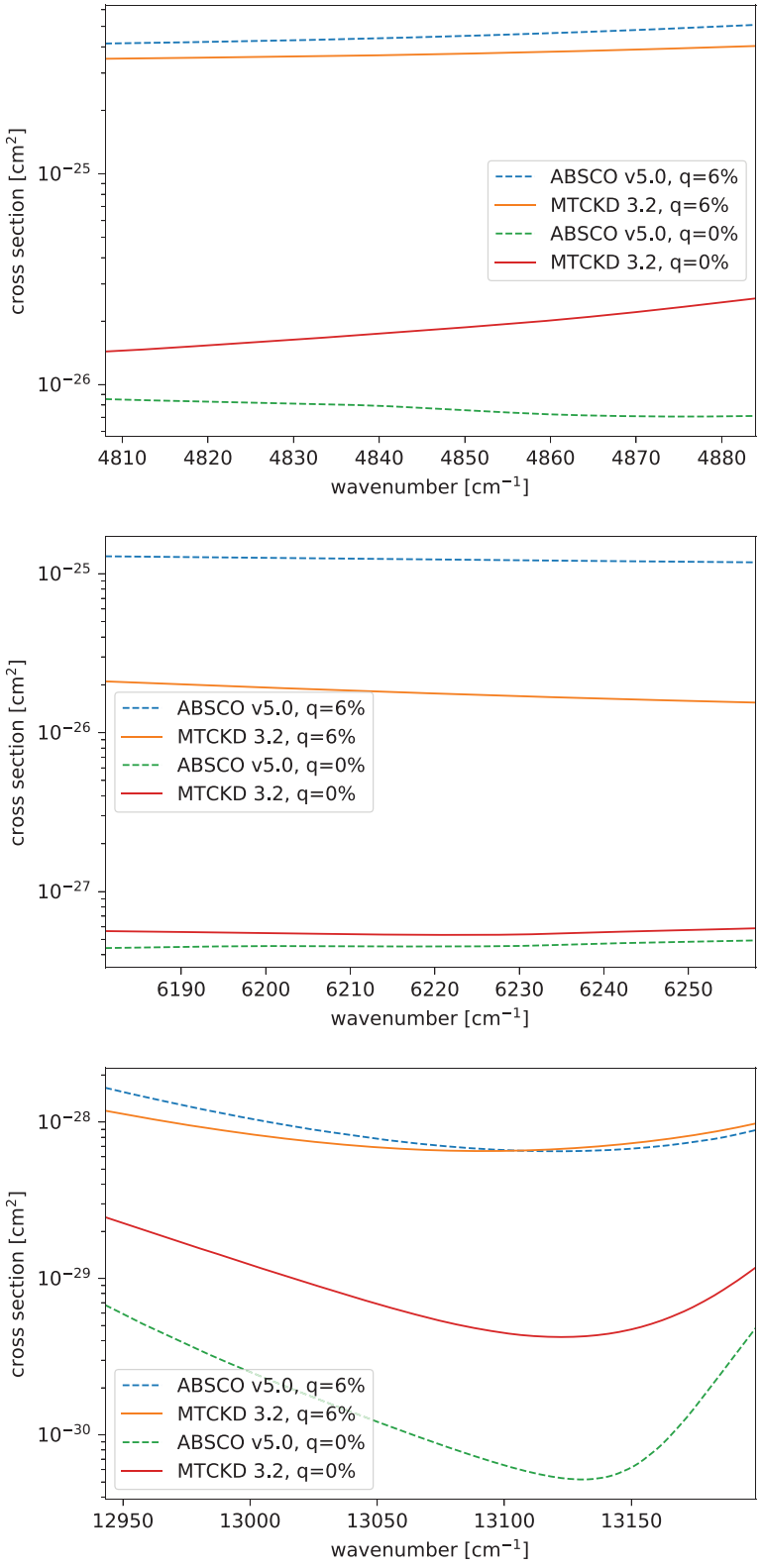

Fig. 1. Continuum cross sections from the MT_CKD models used in ABSCO v5.0 (v2.6) and in ABSCO v5.1 (v3.2) for water mixing ratios (q) of 0% and 6%.

20120705, 20120718). Data selection criteria for a subset of spectra from within these ten days were identical to those used for the [11] study. Briefly, these criteria were: (1) the time series of solar irradiance from NIMFR is consistent with clear skies (cloud free); (2) radiance measurements in the OCO-2 bands are reasonably stable; (3) the precipitable water vapor (PWV), as computed by a retrieval from an ARM microwave instrument [51], varies by less than 10% over a given time period; (4) the aerosol optical depth (AOD) derived from the NIMFR in its 11532 cm^{-1} channel varies by less than 10%; and finally (5) the H_2O airmass factor m_w has a range (max - min) exceeding 1.5. From the ten days, thirteen discrete time periods were selected for analysis and further

Table 2
Level 2 algorithm tests for ABSCO evaluation using OCO-2 soundings.

Label	Description
A: B9 Baseline	B9 algorithm, using ABSCO v5.0 (includes EOFs)
B: B9 No EOF	B9 algorithm, using ABSCO v5.0 (no EOFs included in fits to OCO-2 spectra)
C: H_2O continuum update	As above, with update to H_2O continuum only
D: O_2 and H_2O updates	As above, with updates to both H_2O continuum and O_2 spectroscopy (ABSCO v5.1)
E: B9 with ABSCO v5.1 and EOFs	As above, after re-calculation of EOFs and including these EOFs in the fits to OCO-2 spectra

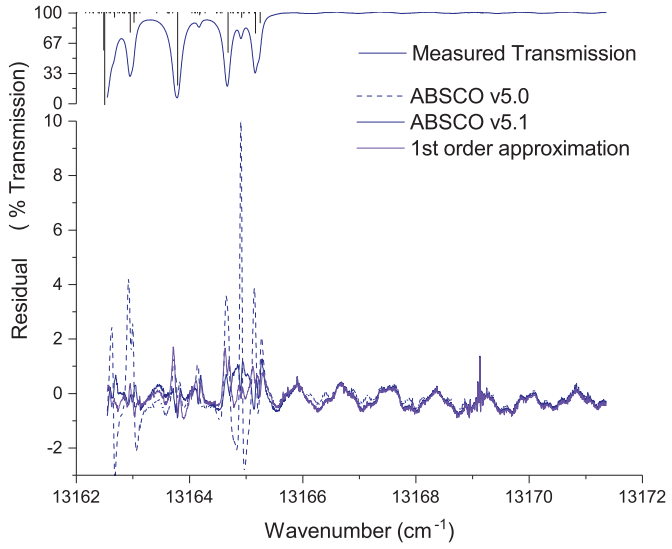

Fig. 2. Measured cavity ring down spectrum segment encompassing the O_2 A-band band-head. The measurement at 1000 Torr (133 kPa) of 0.2% O_2 in N_2 has been normalized for instrument response and converted to transmission, much of the observed etalons are fitted along with the data. Fitted adjustments to the first order model were done only with room temperature data whereas the *W*-matrix component adjustments were done with all data.

filtered to eliminate spectra from consideration if its measurement time coincided with an outlier (more than 20% different than the median for the case) in either the PWV or the AOD measured by the NIMFR. The correction procedure that scales and bins an entire TCCON FTS observation, to match the effective irradiances of temporally matched NIMFR irradiances in wavenumber bins, was again utilized. This vetting process eliminates points that are far from the ideal airmass × vertical optical depth due to instrumental noise and/or aerosol extinction and gives the data the best possible value of vertical optical depth for subsequent determination of unexplained optical depths.

2.2. Evaluation using satellite soundings

With multiple years of OCO-2 mission data in hand, a test set of representative data has been developed for standardized L2 algorithm testing. Results of this work utilize a set of approximately 600,000 OCO-2 "ocean glint" soundings that span most of the time associated with the OCO-2 mission, cover the full range of latitudes, all months for multiple years and solar zenith angles (airmass) viewed by OCO-2, include representative samples from all eight OCO-2 footprints, and have been screened to remove outliers and to select for low aerosol, high confidence retrievals (based on retrieval results from the baseline B9 algorithm). Strictly speaking, the ocean glint soundings also include results from inland water bodies, where the whole surface of any particular footprint is entirely water. For the testing of the impact of the ABSCO updates, we have chosen to focus here on water-surface glint data as this reduces interference from the more complicated situation of land surfaces.

Table 2 lists the L2 algorithm tests for which results will be described in later sections.

2.3. Method and model refinement

2.3.1. Physical model

High resolution spectroscopy is particularly well suited to the determination of line-by-line parameters. However broadband effects are subject to distortions and systematic errors that are different than narrowband effects. The fitting program was previously able to account for these effects with a background polynomial fit; however, a physics-based CIA model was developed in the recent effort to improve parameterization of the O_2 A-band. The details of the model were provided in [11]. In this section we only repeat the portions necessary to express the physical model for the calculations of atmospheric absorption coefficient (ABSCO) tables. The relatively large set of parameters fit simultaneously to determine molecular constants, broadening coefficients, pressure-induced line shift coefficients, line mixing coefficients, and their respective temperature dependences as well as speed-dependence parameters are provided in supplemental tables along with physical descriptions of the values. For monomeric absorption, the program computes the contribution of each quantum transition to the optical depth of each spectrum, or derived table, and sums the values as shown in Eq. (1):

$$\kappa_i = \varrho_{O_2} \sum_{k=1}^{N} [F_k(x_i, y, s) + Y_k(p, T) F_k'(x_i, y, S)] I_k'(J, m, p, T) \quad (1)$$

Where the absorption coefficient κ_i is determined at the *i*th frequency (σ) for all k of the N lines specified in the model and within a cutoff criterion. The partial density ϱ_X for each spectrum is found in Supplemental Table 1, and is fixed for ABSCO table generation. F_k and F_k' are the real and imaginary parts of the speed-dependent Voigt profile, parameterized for pressure dependent line position, x_i, pressure dependent linewidth, y, and speed-dependence, s, the Rosenkranz parameter, Y_k, calculated from the augmented **W**-matrix described later, and finally, $I'_{k(J,m,p,T)}$ is the temperature and quantum state dependent line intensity that can also be modified by pressure-dependent line-mixing. For fitting, the absorption is then converted to transmission using Beer's law; $T_i = e^{-L\kappa_i}$, using the pathlength, L, and O_2 number density, ϱ_{O_2}, for direct comparison to experimental data. For ABSCO table generation, specific values of air pressure and temperature are utilized to populate the table.

We determine the line parameters associated with the pressure dependent lineshape (see Supplemental Tables), for O_2- (self) and N_2-broadened spectra simultaneously at a broad range of pressure (p) and temperatures (T) from different types of instruments (FTS and CRDS). The algorithm uses the van der Waals equation for pure gases to adjust absorber partial pressures to effective partial pressures that account for the corrected number density. For foreign gas mixtures, separate line parameters are determined for the non-absorbing gas effective pressures. Line mixing can be modeled with

the multi-spectrum fitting algorithm as a function of wavenumber σ_i in a matrix form Levy et al. [20] where **W** is the collisional relaxation matrix which represents line mixing amongst the transitions. Significant line mixing occurs for particular groups of transitions rather than for all lines. (i.e., the propensity rules [34]). For the O_2 A-band, Drouin et al. [11] confirmed the NIST sensitivity study (see [23]) that showed that the dominant spectroscopic uncertainties in forward models are associated with LM and CIA, consistent with the results of [7] for CO_2. The first-order approximation to LM may be implemented on the diagonal of **W**, which was done for existing CRDS data [21]. The software is tooled for fitting of both first-order LM and full LM among sets of multiple transitions. For full LM, the **W** matrix that is projected into line-space in Eq. (1) is expanded with subscripts that span Liouville (double) line space:

$$\kappa(\sigma,T) = 8\pi^2[1-e^{-hc\sigma/kT}]\varrho_{tot}x_{O_2}\Sigma_k\Sigma'_k\rho_k(T)d_k d_{k'}Im[<k'|\Sigma(\sigma) - L_0(\sigma) - iW_{kk'}(T)|k>] \quad (2)$$

where the $W_{kk'}$ matrix elements are those for the broadener(s) in the data set, and d_k and d'_k account for quantum and thermal intensity variations within the relaxation matrix and the Σ and L_0 matrices are diagonal functions of the line position that remove the wavenumber dependence from the **W** matrix and allow it to be manipulated spectrum-by-spectrum rather than wavenumber by wavenumber.

In the full line mixing scenario the values of **W** are determined directly in the spectral fitting. Unlike the first-order LM, the results cannot be tabulated line-by-line (e.g., in HITRAN or SDF format), so additional, multidimensional bookkeeping is done for these parameters. In full LM, the 'recommended' values of all of the collisional parameters will become dependent on the off-diagonal elements, meaning that appropriate database storage (e.g. HITRAN) may not accommodate the model. Fortunately, the databases have developed capability to tabulate line-by-line 1st order correction factors, $Y_k(T)$ as shown in Eq. (1) which can be derived from **W** using matrix diagonalization schemes. Utilization of this 1st order approximation as input, however, does ignore the second order effects, which is justified for the majority of the O_2 A-band.

The data collected at NIST was demonstrated to have stronger dependences on foreign (N_2) line-mixing compared with the prior available data. This situation revealed the inadequacy of the assumption in [11] that **W** matrix elements connecting odd J levels were negligible. Consequently, the four sub-band matrices used by Drouin et al. [11], that interconnected RR, RQ, PP and PQ transitions only within each group, were re-cast as a single (70×70) matrix with all possible interconnections explicitly defined.

The CIA spectrum is determined from the difference between the observed spectrum and the sum of all modelled lines (including LM) as shown in Eq. (3).

$$\kappa_{obs}(\sigma,\varrho_{tot},T) = \varrho_{O_2}\kappa_{res}(\sigma,T) + \kappa_{nonres}(\sigma,\varrho_{O_2},\varrho_{N_2},T) \quad (3)$$

This difference may be fitted in the multi-spectrum fitting software with Chebyshev polynomials, however such a method makes a common physics model difficult to implement. To improve this situation, the CIA forward model described in [11] was implemented with modified inputs. In this model CIA for each pair of gases is defined by the components at each frequency for each spectral data point are calculated, the program then incorporates this contribution into the baseline (or background) of the calculated transmission spectrum.

$$\kappa_{nonres}(\sigma,\varrho_{O_2},\varrho_{N_2},T) = \varrho_{O_2}\varrho_{O_2}\alpha(\sigma,T)_{O_2,O_2} + \varrho_{N_2}\varrho_{O_2}\alpha(\sigma,T)_{N_2,O_2} \quad (4)$$

To enable theoretical modeling of the underlying (and always unresolved) spectral structure of the CIA, the $\alpha(\sigma, T)_{X,Y}$ coefficients are built up from a list of individual frequencies, intensities and linewidths (for each gas pair), rather than a predetermined list of CIA cross-sections at each frequency.

2.3.2. Analyses of laboratory spectra

The new CRDS spectra with nominally 0.2% and 2% O_2 in N_2 at T = 237 K to 290 K, described in Supplemental Table 1 were incorporated into the multi-spectrum fitting tool in logical blocks that enabled systematic vetting of experimental conditions associated with the new experimental methods. CRDS data from the temperature controlled cell, recorded as segmented sections between optically thick resonant features, were found to have a high degree of consistency within a pressure/temperature/mixing ratio set, with a few exceptions. Within these sets systematic offsets in the frequency and intensity axes were observed. For frequency calibration, the initial spectra recorded are in agreement with prior line positions [11] within experimental error, whereas all subsequent spectra recorded and analyzed in this study require a single systematic offset of 20 MHz. Additional attention to the intensity axis was required to bring the new data into accord with the legacy data, with offsets of around 0.5%, resulting in significant changes to band intensity retrievals that could not be reconciled. The new spectra, having an extensive dynamic range in the pressure and temperature variables, but with only a weak dependence on pure O_2 properties, were deemed to be more valuable for their relative lineshape and CIA information, and the intensity information was disregarded in the fitting procedure through simultaneous fitting of a transmission background (100% T) and zero offset. Subsequent experiments at NIST [13] have revealed, and mitigated, small intensity offsets associated with digitization electronics, such that future measurements may be free of these biases. With the adjustments described above, the new data was incorporated into the prior data model and utilized to further refine the physical model of O_2 A-band absorption. Due to the caveats outlined here, the present re-analysis should be regarded as an improvement in the relative consistency of O_2 A-band lineshapes and CIA, and not as an incremental improvement in the absolute intensities or line positions.

The most dramatically presented information in the new spectra was observed in the pressure-, temperature-dependent *R*-branch band-head data, where deviations from the prior model were as high as 10% T (see Fig. 2). Inspection of the residuals and their dependence on the quanta and neighboring features revealed discrepancies in both the high-*J* intensity model as well as the line-mixing model. Because these effects are correlated (when using full line-mixing), care was taken to intercompare the high-*J* transitions in both the *P* and *R* branches, where line-mixing (and 2nd order intensity) effects might be strong in the band-head of the *R*-branch, the effects would be muted at the same *J* values in the *P*-branch where differences in transitions energies (the denominator of $W_{kk'}$) would be relatively large. This inspection revealed an overlooked inconsistency between the FTS and CRDS *P*-branch intensities in prior work of several percent, as well as a similar inconsistency between the 'new' CRDS data and the prior CRDS data in this same region, also several percent. The intensity discrepancy at high *J* was symmetric, *i.e.* the higher *J* lines in both branches were found to be weaker than previous determinations. Since the discrepancies between the CRDS datasets straddled the (lower SNR) FTS data, it was decided to retain both datasets with equal weights for further fitting. The prior CRDS data did not cover the *R*-branch, such that some bias in the band-head region may linger in the present analysis.

With the intensities in the *R*-branch better determined, significant residuals remained that can be largely attributed to the expected line-mixing effects in the band-head region. Attempts to fit nearest neighbor ($\Delta J = \pm1$) and next nearest neighbor (ΔJ

$= \pm 2$) values in the **W** matrix were challenging due to strong inter-dependencies on other values in the full matrix, many of which have non-negligible contributions in the band-head. To address this issue, the theory [50] was again leveraged in the multi-spectrum fitting program. Since the new data was not strongly dependent on pure-O_2 line broadening/mixing, the assumptions for O_2-O_2 line-mixing (from [11]) were kept fixed, but the assumptions for O_2-N_2 line mixing were systematically tested to determine the relative importance of $\Delta J = \pm 1, \pm 3, \pm 5...$ and $\Delta J = \pm 2, \pm 4, \pm 6...$ components. The tests involved variation of coefficients that multiply all of the even and odd components of the theoretical line mixing values and subsequent inspection of residuals with spectral parameters (as in prior work). The tests indicated that the sharp, line-by-line residuals, were affected in complex ways, and that the slow band-wide effect, that is ascribed to CIA, could become unphysical (i.e. negative absorption) without proper balancing of the effects. An optimal balance of the odd and even W-matrix coefficients was found with $-0.65W_{j,j+2n}$ and $0.20W_{j,j+2n+1}$ for the present data sets. Optimal in this determination was a subjective comparison of the resultant broadband (CIA) changes combined with improvements in the narrow-band (line-by-line) residuals in the band-head region. Subsequent to determination of these empirical scaling parameters for the theoretical line-mixing, systematic tests to fit individual off-diagonal elements of the **W**-matrix were performed. Thirty-nine fitted values of these **W**-matrix elements were retained if the fit residual improved and the fitted values were bounded by the magnitude of associated broadening elements, which must be larger by definition. Correlations of **W**-matrix elements with broadening and shift parameters within the band-head were tracked and mostly chosen to conform with the expected smooth *J*-dependences observed at similar *J*-values in the *P*-branch.

Adjustments of the O_2-N_2 line-mixing had concomitant effects on the residual absorptions that are attributed to CIA. The changes were most pronounced in the high-pressure air data from legacy CRDS *P*-branch measurements, which had been shown to be in close agreement with atmospheric data [11,23]. Adjustments to the laboratory model of O_2-N_2 CIA resulted in a broader *P*-branch CIA in closer agreement with recommended values [49,50] prior to [11] and in better agreement with theory [15,16] which had disputed the physical correctness of the narrower CIA presented in [11]. The effects of the new O_2-N_2 line-mixing upon the *R*-branch CIA were not as easily discerned, mostly because the effects of O_2-O_2 line-mixing and CIA must also be disentangled. Attempts to model higher O_2 mixing ratio CRDS spectra were hampered by these unknowns and the data value was found to be limited by the difficulty in assessing the systematic errors discussed earlier. At this point in the effort, initial spectra from the high-pressure FTS experiment [45], which is similar in nature to the experiments by Tran et al. [50], became available and served to mitigate unknowns associated with the O_2-O_2 CIA in the present analysis. For estimation of the O_2-O_2 CIA in the entire A-band region, the highest pressure pure O_2 spectrum from Sung et al. [45] was input into a copy of the multi-spectrum fit containing the physical model presented here. Execution of the program with no CIA, fixed line-by-line parameters, and unitary transmission background results in residuals demonstrative of the residual, non-resonant absorption in a given spectrum. Off-line analysis of this residual resulted in a CIA in much closer agreement with [50] than with [11]. An intercomparison of the present O_2-O_2 CIA with Tran's recommendation, is shown in Fig. 3; a comparison with raw residuals from the experiment/resonant line model reveals a close match in magnitude and breadth of these features, but some variability in the sharp features. The double-peaked feature in the residual and our present air model, is likely due to remaining inconsistencies in the N_2-O_2 LM. This assumption has only a minor effect on the results at > 25 cm^{-1} from the band-head, and will be investigated more fully in a follow-up effort that utilizes all of the data reported in [45].

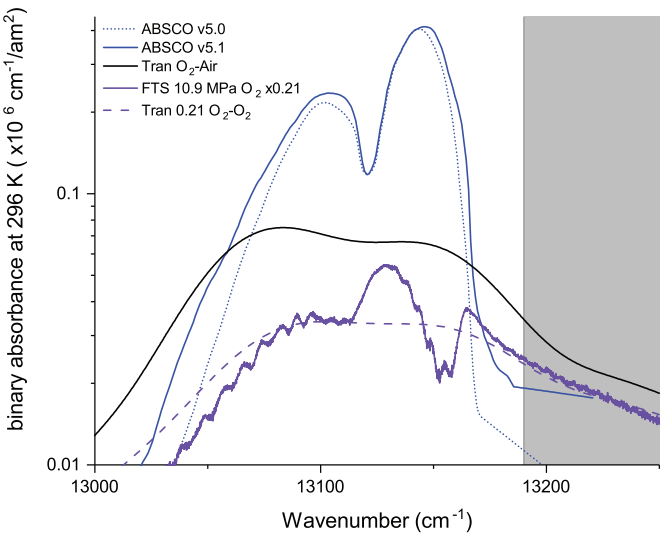

Fig. 3. Collision induced absorption (CIA) of air used in ABSCO v5.1 (solid blue) and ABSCO v5.0 (dotted blue) and that available in HITRAN from [50] (thick black). The non-grey area indicates the ABSCO table region. Pure O_2 CIA and a residual from the 10.9 MPa (109 bar) pure O_2 FTS spectrum scaled to amagat units and multiplied by the O_2 air fraction are shown for comparison. CIA in the peaks is compressed in long path transmission spectra, reducing some concern over the large discrepancies in the narrow features. The present ABSCO 5.1 update focused on the absorption below 0.1×10^{-6} cm^{-1}/am^2 in the wings, where the agreement with Tran et al. [50] is improved.

The analysis of the laboratory data provides a strong, experimentally traceable, physical model for atmospheric absorption. However, testing of the model with atmospheric spectra indicated lingering inconsistencies in the line-mixing and CIA models. Therefore, for ABSCO v5.1 in the O_2 A-band, we have continued to use the approach described in [11] for ABSCO v5.0, combining line-mixing and line parameters derived using laboratory spectra with a CIA that is empirically derived from the atmospheric residuals.

The method developed in [11] for extraction of CIA from co-located TCCON and NIMFR instruments at the DoE Southern Great Plains site in Lamont, OK was again applied to minimize the discrepancies that result from extrapolation of the laboratory data to high air-mass field conditions. The process, which utilized the experimentally refined intensities and line mixing, resulted in a CIA that retained the sharp central peaks determined in [11], but with wings that were closer to the earlier work of [50]. We note that the peaks in the present CIA correspond to the most optically thick portions of the atmospheric absorption, which increases the uncertainty in the absorption coefficients but also means that the impact of any error on the retrievals arising from these peak regions is minimal.

3. Results: impacts on fits to laboratory and TCCON spectra

3.1. Oxygen A-band spectral analysis

In the laboratory data, the changes in high-*J* transition intensities are observed as conflicting residuals in the two sets of CRDS *P*-branch data, but as reduced residuals in the FTS *P*-branch regions. We note that the FTS spectra appear to indicate intensity values between these two particular CRDS data sets and that the present fit agrees best with the FTS data here. In the *R*-branch band-head region, the intensity change reduced the largest residuals (see Fig. 2) even before line-mixing components were allowed

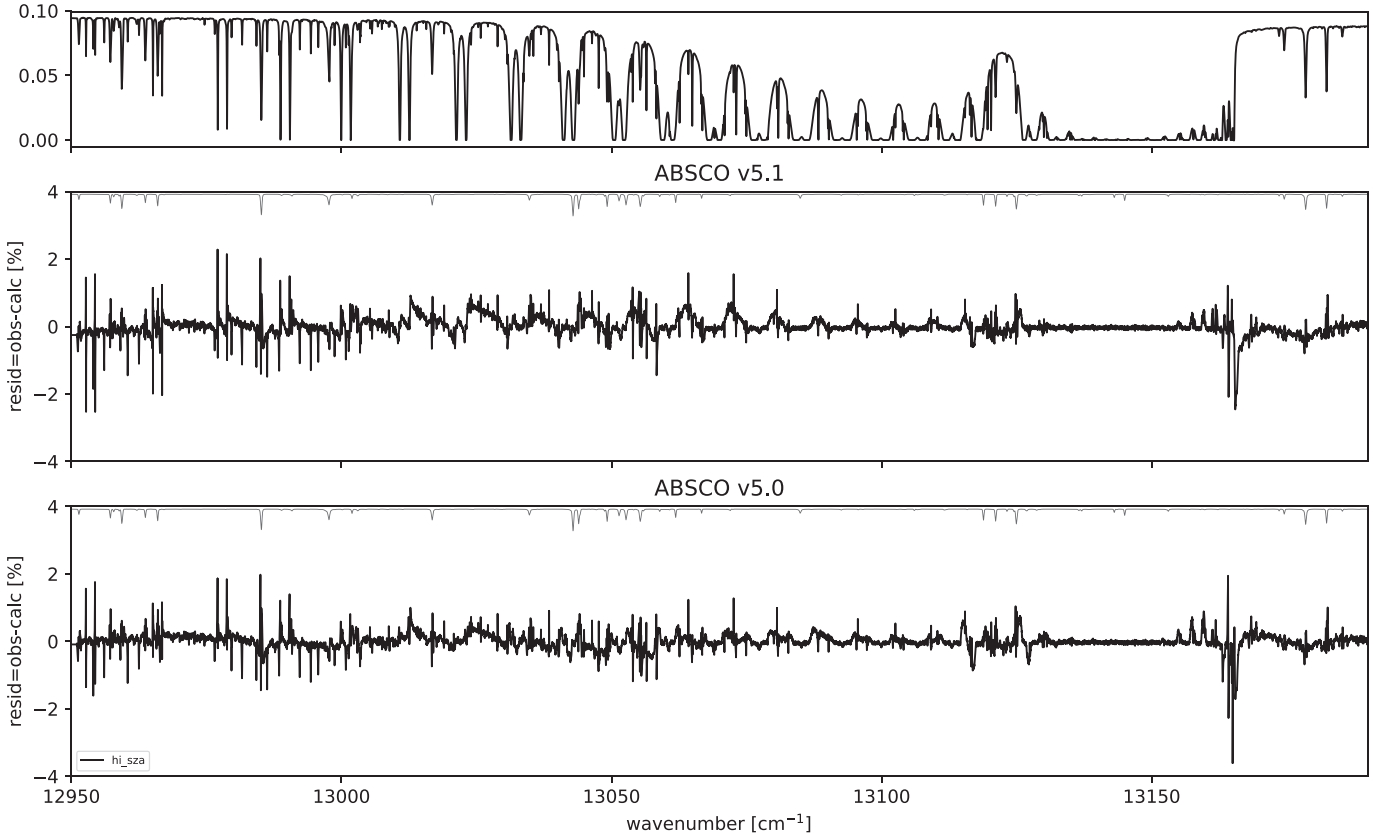

Fig. 4. High airmass (solar zenith angle $>$ 75^o) residuals for ABSCO v5.0 and ABSCO v5.1. Top panel shows the average spectrum. Middle panel shows averaged spectral residual from ABSCO v5.0, after fitting of surface pressure. Lowermost panel shows the residual from fits using ABSCO v5.0. Residuals near the band-head are reduced in ABSCO 5.1, while *P*-branch residuals have increased slightly.

to vary. The residuals in all of the laboratory data for the band-head region are further reduced by the line-mixing adjustments in this effort.

The O_2 spectroscopy changes are observable in both the laboratory fitting and TCCON residuals in comparable ways. However, the impacts are somewhat different owing to the underlying physical conditions being fixed for laboratory work and variable in the remote sensing data. Analysis of TCCON data using carefully selected data that is free from aerosol and cloud perturbation validates the indicators from the laboratory analysis in that the residuals in the band-head region (13160 cm^{-1} - 13170 cm^{-1}) are significantly reduced and those in the *P*-branch (13050 cm^{-1} -13100 cm^{-1}) are similar in magnitude, but different in shape. Fig. 4 displays averaged high-airmass (solar zenith angle $>$ 75*o*) residuals for the TCCON data used to evaluate ABSCO v5.1 vs ABSCO v5.0. High airmass cases show the largest residuals were noted. Fig. 4 shows a clear reduction in the magnitude of the ABSCO v5.1 residuals in the region of the band-head relative to ABSCO v5.0, consistent with the laboratory fits. However, residuals between *P*-branch doublets are slightly larger in ABSCO v5.1 compared to ABSCO v5.0. Due to the method of retrieving CIA from similar TCCON data, it is not expected that much of the residuals observed here would be due to CIA errors. However we note that preliminary CIA coefficients derived solely from laboratory spectra were not in agreement near the strongest absorption where the uncertainties in the methods all increase. The sawtooth nature of the *P*-branch residuals suggests that there is still scope for improvement in the representation of line mixing for O_2.

Fig. 5 shows the residual rms for ABSCO v5.0 and ABSCO v5.1 as a function of airmass for the full set of Lamont TCCON spectra used. The rms quantity plotted here is the root mean square of (R_{meas} - R_{calc}) / max(R_{meas}) where R_{meas} and R_{calc} are the measured and calculated radiance spectra. Residuals are separated here by season. Winter/spring cases differ from summer/spring cases by both temperature and humidity ranges. The drier winter cases shows residuals that are relatively flat with airmass. The residual rms shows only modest changes with airmass when comparing the full ABSCO v5.0 (blue) and ABSCO v5.1 (green) results, with the most notable improvement at 1–5 airmass. The rms for the lowest airmass residuals is dominated by features in the band-head, such that this improvement may be largely attributed to the changes in that portion of the spectral model. At higher airmasses for the winter data, the changes in LM/CIA seem to largely cancel out in this metric. In the summer/spring rms, the scatter at high airmass makes any conclusions about changes circumspect. However, a reduction of rms at low airmass for ABSCO 5.1 is observed. A clear trend of increasing rms with airmass is seen in the warmer and wetter summer data. The reason for this is not currently well understood, but will be a topic of ongoing investigation.

3.2. Oxygen A-band geophysical variables

Spectral residual changes (and rms) were not the only criteria for evaluation of ABSCO table changes. Impacts on retrieved surface pressure were also evaluated. At the TCCON site in Lamont OK, surface pressure is continuously recorded, allowing systematic comparisons of retrieval results against ground truth. Fig. 6 shows differences between retrieved values of surface pressure and those measured directly at the Lamont station, as a function of airmass, for single-band retrievals using ABSCO v5.0 and ABSCO v5.1.

Results in Fig. 6 are split into two temperature bins, according to the 700 hPa temperature above the Lamont site (greater than

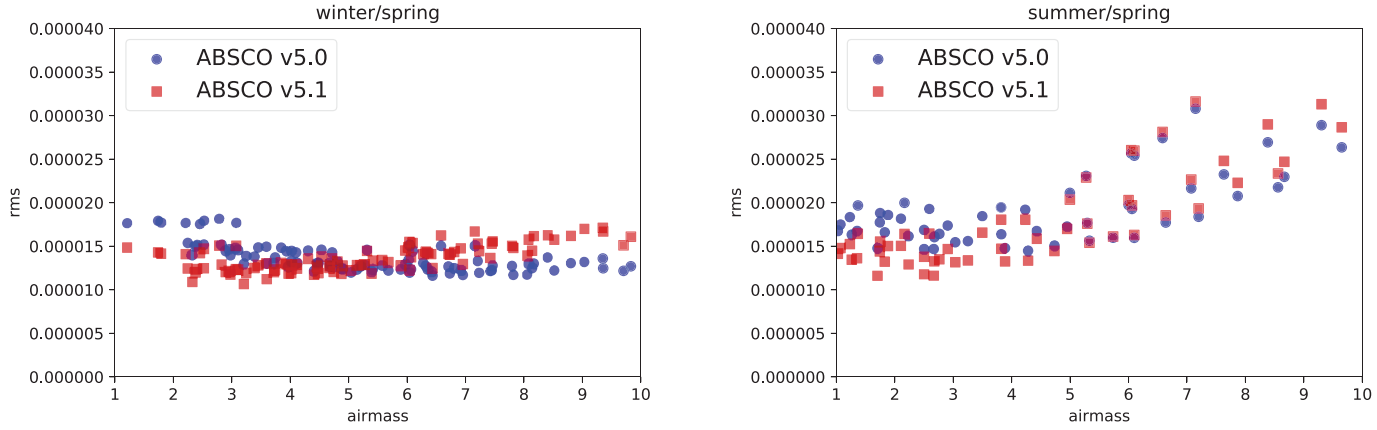

Fig. 5. Residual rms for fits to TCCON spectra as a function of airmass.

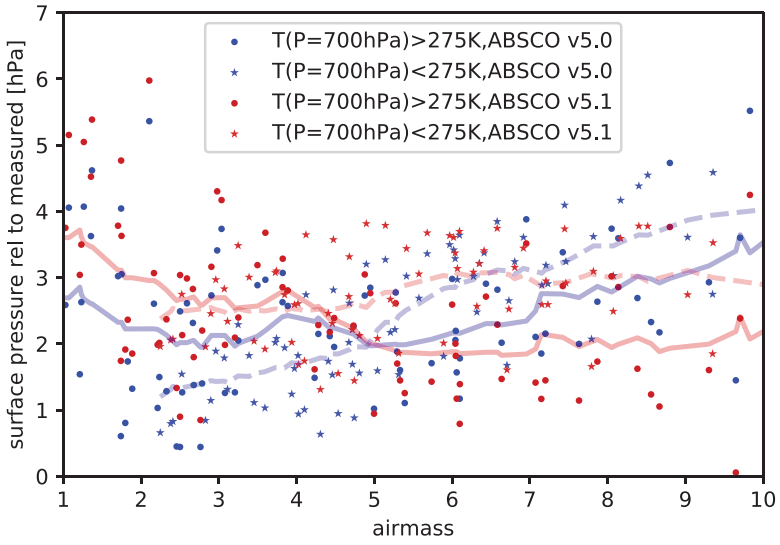

Fig. 6. Comparison of ground-based surface pressure retrievals for ABSCO v5.0 and ABSCO v5.1 as a function of airmass with respect to ground-based truth. Data are partitioned into high and low temperature measurements, where a temperature of 275K at 700 hPa separates the two categories. Moving averages over 1 airmass halfwidth bins are shown for both high (solid) and low (dashed) temperature datasets.

or less than 275 K). The ABSCO v5.1 results in closer agreement between temperature bins at low airmass and a greater separation between temperature bins at high airmass compared to ABSCO v5.0. It is interesting to note that there was no explicit change in temperature dependence parameters for line parameters or line mixing between the two ABSCO versions. The change in temperature dependence of retrieved surface pressure appears to be an indirect impact of the changes in the O_2 line mixing.

We note here that the results of these surface pressure retrievals were utilized in the determination of the empirical O_2 CIA. The changes in residuals between 13,050 cm^{-1} - 13100 cm^{-1} (in the heart of the *P*-branch) were a compromise that helped determine the relative amounts of line-mixing and collision induced absorption in this range. The compromise was reached by observing effects on the bias in the surface pressure retrievals. While inspecting the range of empirical line-mixing scaling factors and the effect on CIA, as well as the impact of these adjustments on TCCON retrievals, it was observed that the CIA has a particularly strong impact on retrieved products in the region of the resonant *P*-branch lines where the intensity is dropping, *i.e.* at the intensity inflection points. Also while making the adjustments to empirical line mixing and collision induced absorption, the behavior or the CIA was checked at the low pressure limit (in that residuals that were being improved at high pressure did not correspond to opposing residuals at low pressure), and the effect of adjusting the intensity cutoff for calculation of resonant lines was confirmed to have no effect on laboratory residuals. The relative increase in CIA past the band-head is not easily observed in the TCCON spectral residuals, partially because the changes are offset by additional line-mixing in the band-head as well as reduced intensities of the lines near the band-head. Like the observation in the *P*-branch, this region is an inflection point in the resonant line intensities, and thus enables changes in the CIA to more strongly influence retrievals of geophysical variables.

3.3. Impact of water vapor updates

The update to the H_2O continuum between ABSCO v5.0 and v5.1 did not impact either the residuals or the single-band XCO_2 retrievals from this set of Lamont TCCON spectra.

4. Results: impacts within OCO-2 level 2 algorithm

4.1. Impacts of combined water and oxygen updates on OCO-2 residuals

The OCO L2 algorithm uses an optimal estimation approach Rodgers [38]. Further details of the algorithm and the configura-

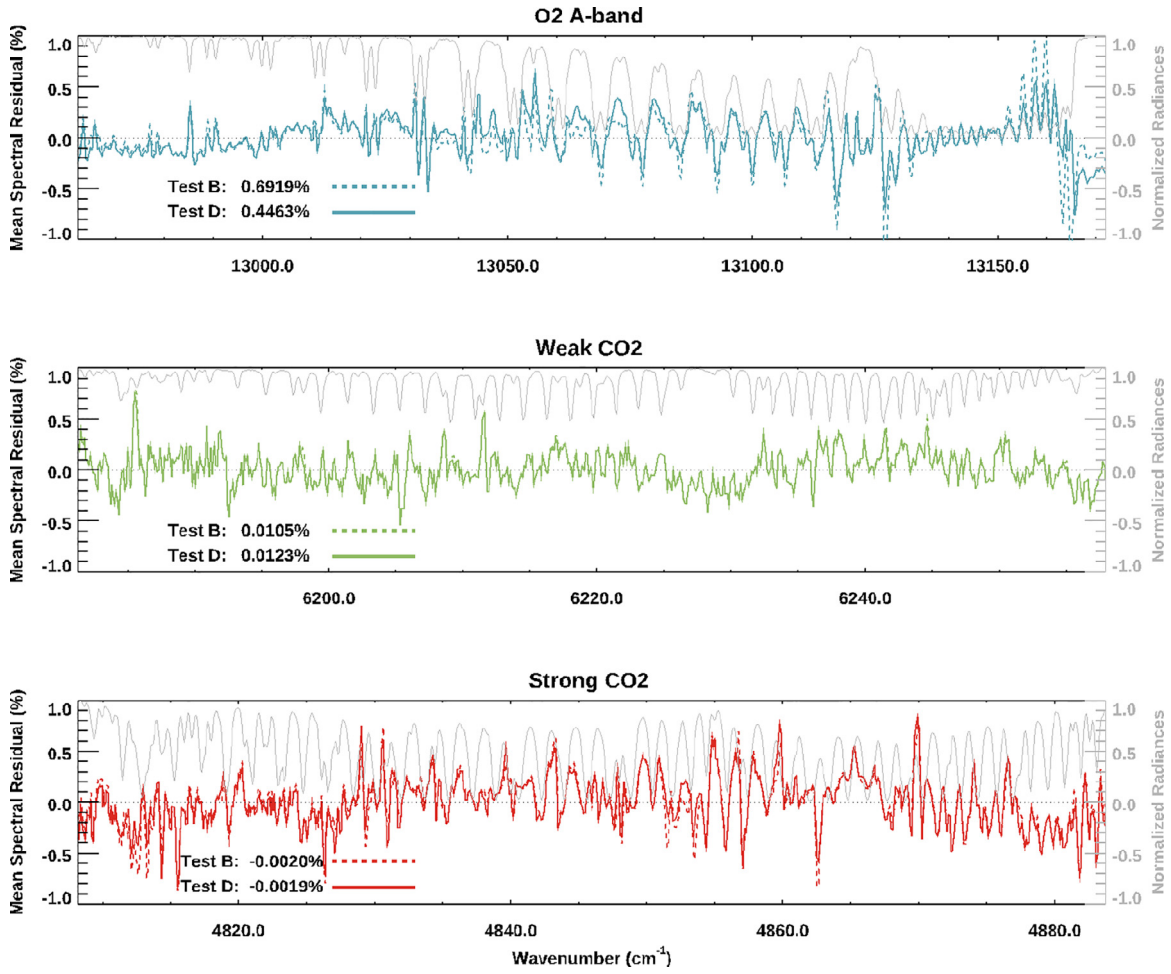

Fig. 7. Averaged OCO-2 spectral residuals for the 0.76 µm O_2 A-band (upper panel), the 1.6 µm weak CO_2 band (middle panel) and the 2.06 µm strong CO_2 band (lower panel). Gray solid lines show averaged radiance spectra for each band. Solid colored lines show the residuals for Test B (ABSCO v5.0, no EOF) while dashed lines show residuals for Test D (ABSCO v5.1, no EOF, which includes updates to both the O_2 spectroscopy and the H_2O continuum model).

tion of the state vector can be found in O'Dell et al. [32] and references therein. In this section we examine the results of L2 test sets for ocean/glint cases with respect to the radiance residual statistics (mean and rms), as well as the χ^2 parameter that describes the goodness of fit.

Fig. 7 presents average measured radiances and mean residuals (see supplemental material for the residual standard deviation) for the ocean/glint test cases B and D described in Table 2. The radiances show the band structure of the O_2 and CO_2 absorption.

The differences in mean radiance residuals between ABSCO v5.0 and ABSCO v5.1 are most prominent in the O_2 A-band, where significant changes to the line-mixing and CIA models result in differences between the sharp features, particularly near the band-head. There is also a significant change beyond the band-head where the CIA adjustment results in a significant shift in the baseline. Minimal differences are visually discernable in the weak and strong CO_2 bands where the spectral line models are unchanged, reflecting the fact that the water-vapor continuum update is broadband in nature over these bandwidths. Small impacts of broad-band radiance model changes are reflected in the χ^2.

Non-linear least squares fits can be evaluated statistically with the χ^2 parameter that is ideally unity for exact, constrained, parametric fits, but tends to values greater than one for noisy, partially constrained and correlated parametric fits. For a large ensemble of observations, χ^2 values tend to fall within a range characteristic of the model capability to parameterize the data. Outliers in such a distribution indicate model or data inadequacies. Table 3 and Fig. 8

Table 3
Results of retrieval algorithm tests associated with the no-EOF ABSCO v5.0 (Test B), the H_2O continuum update (Test C) and the combined updates for ABSCO v5.1 (Test D), as represented by χ^2 mean ± standard deviation.

	O_2 A Band	Weak CO_2	Strong CO_2
Test B	4.36 ± 1.25	3.20 ± 0.86	3.59 ± 1.55
Test C	4.39 ± 1.26	3.10 ± 0.77	3.36 ± 1.54
Test D	2.88 ± 0.78	3.09 ± 0.76	3.40 ± 1.55

depict the behavior of the χ^2 values for the ABSCO v5.0 (test B, no EOF), incremental ABSCO update with water continuum update (test C) and the full ABSCO v5.1 update (test D). The numerical values shown in Table 3 represent the mean and standard deviation of the χ^2 values in the given band.

The χ^2 behavior changes most dramatically for the O_2 A-band in Test D, which is noticeable as a narrowing of the histogram with a significant decrease in the mean value. Numerically, this is a 38% reduction in the distribution, and a 44% improvement towards an ideal χ^2. This statistical improvement is reflected also in L2 products which depend critically on the retrieval of O_2 column densities, these will be detailed in the following section. Much more modest improvements in χ^2 are observed in the weak and strong CO_2 bands due to the implementation of H_2O continuum updates. Statistical improvements of 5% and 9% towards ideal χ^2 values result for the weak and strong CO_2 bands respectively.

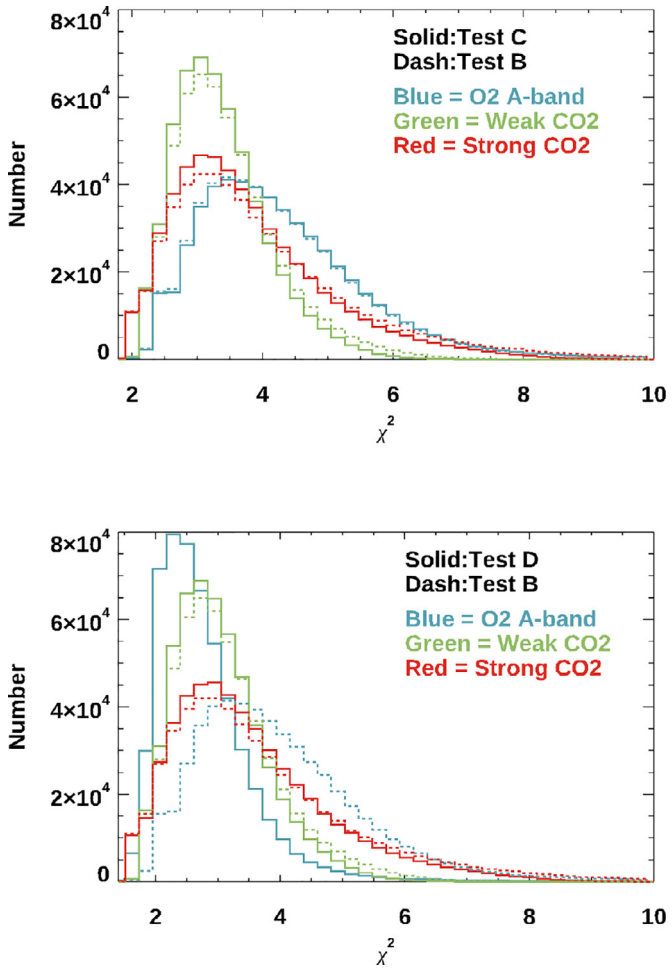

Fig. 8. These two plots show the successive impact of the H_2O continuum update (test C relative to test B) and the O_2 update (test D relative to test B) on the retrieval χ^2 fits.

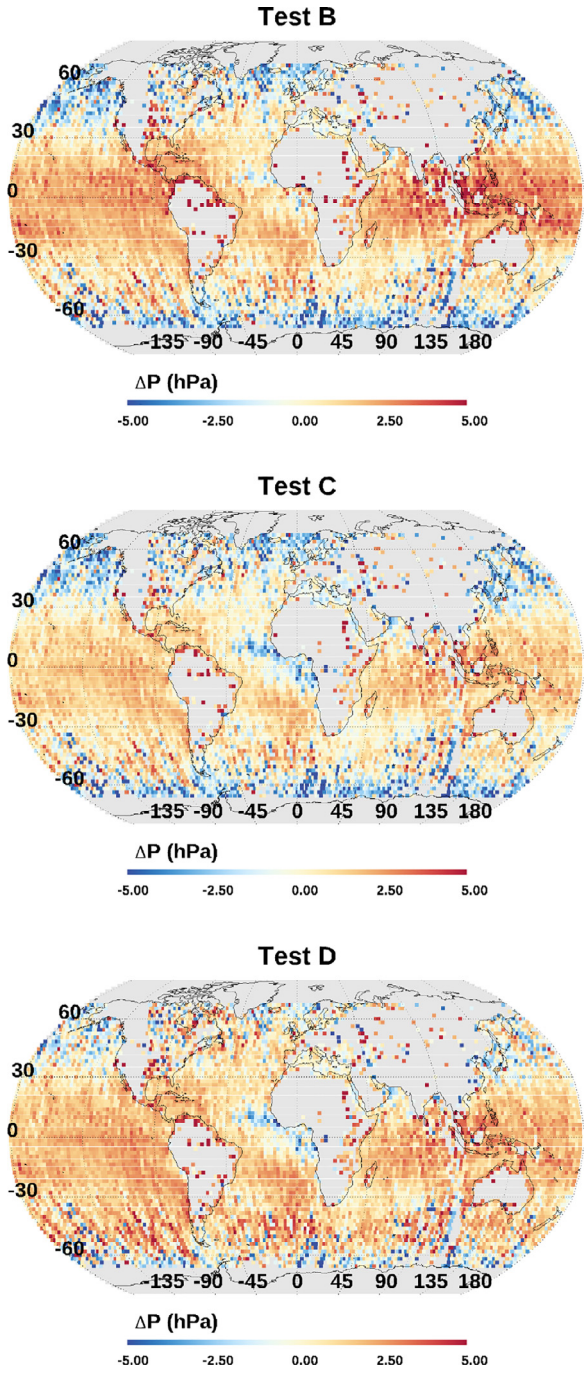

Fig. 9. Maps of mean ΔP for Tests B through D, as defined in Table 2. Test C (H_2O continuum update) reduces high bias, particularly in the Tropics, while test D (O_2 spectroscopy update) reduces the overall latitudinal gradient.

While H_2O is not the main product for the OCO missions, the CO_2 bands are sensitive to changes in tropospheric H_2O. The OCO L2 algorithm does include an H_2O scaling factor in the state vector. This scaling is applied to the initial guess meteorological profile for H_2O, and the scaled profiles can be used to calculate total column H_2O. Nelson et al. [29] showed that these column values compare well against a range of validation measurements from radiosondes and ground-based instrumentation. More recently, Kulawik et al. [18] have shown the potential benefit of retrieving profile H_2O from the OCO missions. Therefore, H_2O spectroscopy is a topic of ongoing interest for the OCO missions, both in terms of impact on the XCO_2 retrievals and in terms of an H_2O product. While validation of H_2O products is outside the scope of this work, the tests shown here indicate that the continuum model (not only the line parameter database) has an impact.

4.2. Impacts of combined water and oxygen updates: geographical variation

In addition to these impacts on residual fits, in the absence of the use of EOFs in the retrievals, the spectroscopy updates have significant impacts on the retrieved parameters. Here, we focus on the retrieved surface pressure and XCO_2. Fig. 9 shows the bias in retrieved surface pressure (ΔP) from the OCO-2 algorithm relative to the Goddard Earth Observing System version 5 Forward Processing for Instrument Teams (GEOS-5 FP-IT) near real time products surface pressure values used as prior information in the OCO-2 retrievals for no-EOF, ocean glint retrievals from tests B,C, and D. The color scale of Fig. 9 indicates OCO retrieved surface pressures that are larger than meteorological priors (GEOS-5 FP-IT) as warm colors and surface pressures that are smaller than priors as cool colors. We assume here that the prior surface pressure values are, on average, a good approximation of truth, and that biases in the OCO-2 retrieved surface pressure values relative to prior result from systematic errors in the forward model. The ABSCO v5.0 no-EOF results (Test B) show a pronounced latitudinal gradient in the surface pressure bias, with an overall negative bias at high latitudes and an overall positive bias in the Tropics. As discussed in

O'Dell et al. [32], this zonal structure in the surface pressure bias is also present in the OCO-2 retrievals when EOF scaling factors are included in the retrieval state vector (not shown in Fig. 9). This will be discussed further in the next section. The water continuum update (Test C) is seen to mute the previously high-biased values in the tropics, while the O_2 A-band update shifts the distribution toward higher surface pressures.

The expectation is that most of the information on retrieved surface pressure comes from the O_2 A-band, but there is also dependence of this quantity on the moist and dry-air continua. The second panel in Fig. 9 shows that the H_2O continuum update, leads to non-negligible changes in the retrieved surface pressure within the OCO algorithm, at least in this no-EOF case. Difference plots, with changes to the surface pressure bias between tests, $\delta\Delta P = \Delta P(X) - \Delta P(Y)$, are shown in Fig. 10. This result was not something that was anticipated in advance. The strongest impacts are seen in the Tropics, in the regions of the globe with the highest column H_2O values. With the cooler color representing a negative shift in a value that was positively biased, the H_2O continuum update is shown to reduce the positive bias around the Tropics (see Fig. 9 first two panels). Fig. 9 also shows the strong impact of the O_2 spectroscopy update on the retrieved surface pressure. Again, difference plots are shown in Fig. 10. The impact of the O_2 spectroscopy update was global and it flattens out the zonal (latitudinal) structure in the initial surface pressure bias, making the bias more uniformly positive with latitude. Reduction in regional dependence of the bias is seen as a positive impact and connected to the reduced breadth of the χ^2 distribution for O_2 A-band retrievals. O'Dell et al. [31] had suggested that one possible underlying cause of the zonal structure in the surface pressure bias could be an issue with the temperature dependence of the ABSCO v5.0 O_2 cross-sections. We note here that in this update between ABSCO v5.0 and ABSCO v5.1, there was no significant change in the temperature dependence of any of the O_2 parameters.

The third and fourth panels of Fig. 10 show the associated changes of the XCO_2 product with the aforementioned test cases. Clearly, the changes due to the H_2O continuum update (Test C- Test B) are comparable in magnitude to the changes in surface pressure, but with a negative correlation due to the influence of the retrieved surface pressure on the XCO_2 quantity. A similar conclusion can be made regarding the O_2 A-band test inter-comparison. These tests, and geometric correlations of the results, indicate that the H_2O update in the CO_2 bands has primarily an effect of the on the surface pressure retrieval, and little effect on the CO_2 column itself. The fact that the amount of column CO_2 (before ratioing to column O_2) is invariant in these tests is not unexpected since the spectroscopic parameters for CO_2 absorption were not changed in these tests.

4.3. Impacts of combined water and oxygen updates: variation with geophysical variables

Finally, we explore the same algorithm tests discussed in the previous sections using two-dimensional histograms that represent the climatological space covered by temperature and H_2O. In Section 4.2 the geophysical variables are shown to correlate with latitude, however, temperature is also strongly dependent on latitude. To explore the effects of our ABSCO table updates with respect to physical variables, the retrieved surface pressures were binned by temperature at 700 hPa (in 2 K increments), total column water vapor, in 2 kg/m^2 increments), and by airmass (in 0.1 increments), all based on meteorological prior re-analysis fields. The mean ΔP (the difference between the retrieved and *a priori* surface pressure, as in Fig. 9) is computed for each two dimensional histogram bin. Applying this procedure to build 9 baseline (Test A - ABSCO v5.0 tables with ABSCO v5.0-based EOFs) re-

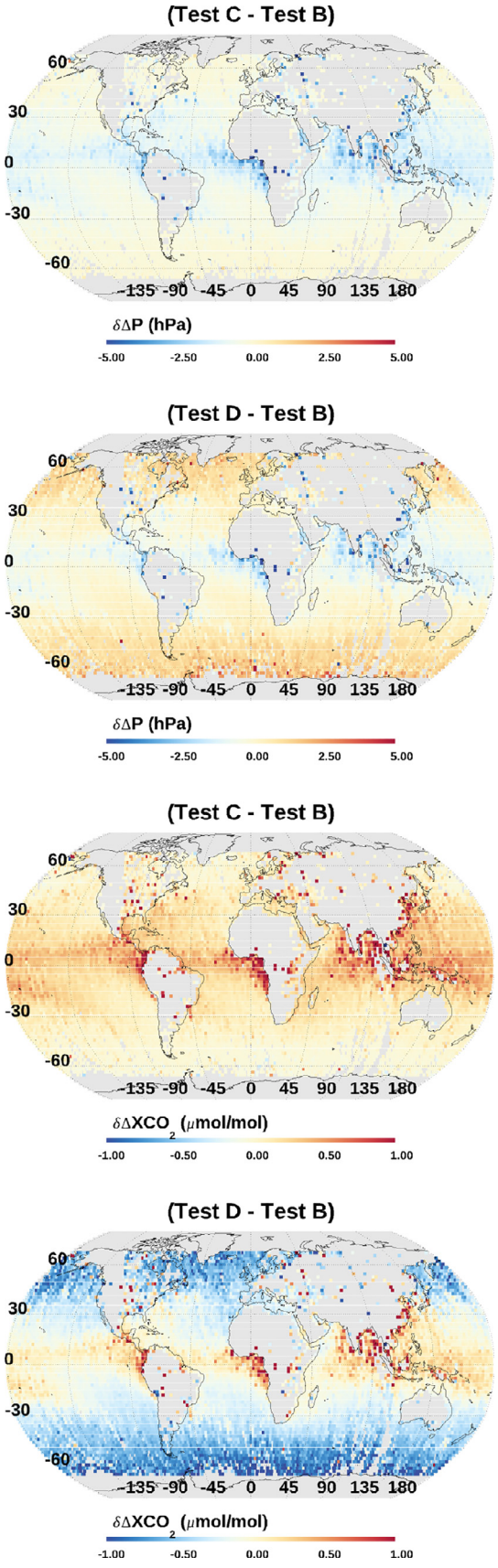

Fig. 10. Impact of H_2O continuum (Test C - Test B) and additional O_2 spectroscopy (Test D - Test B) updates on retrieved ΔP and XCO_2 for the ocean glint test set.

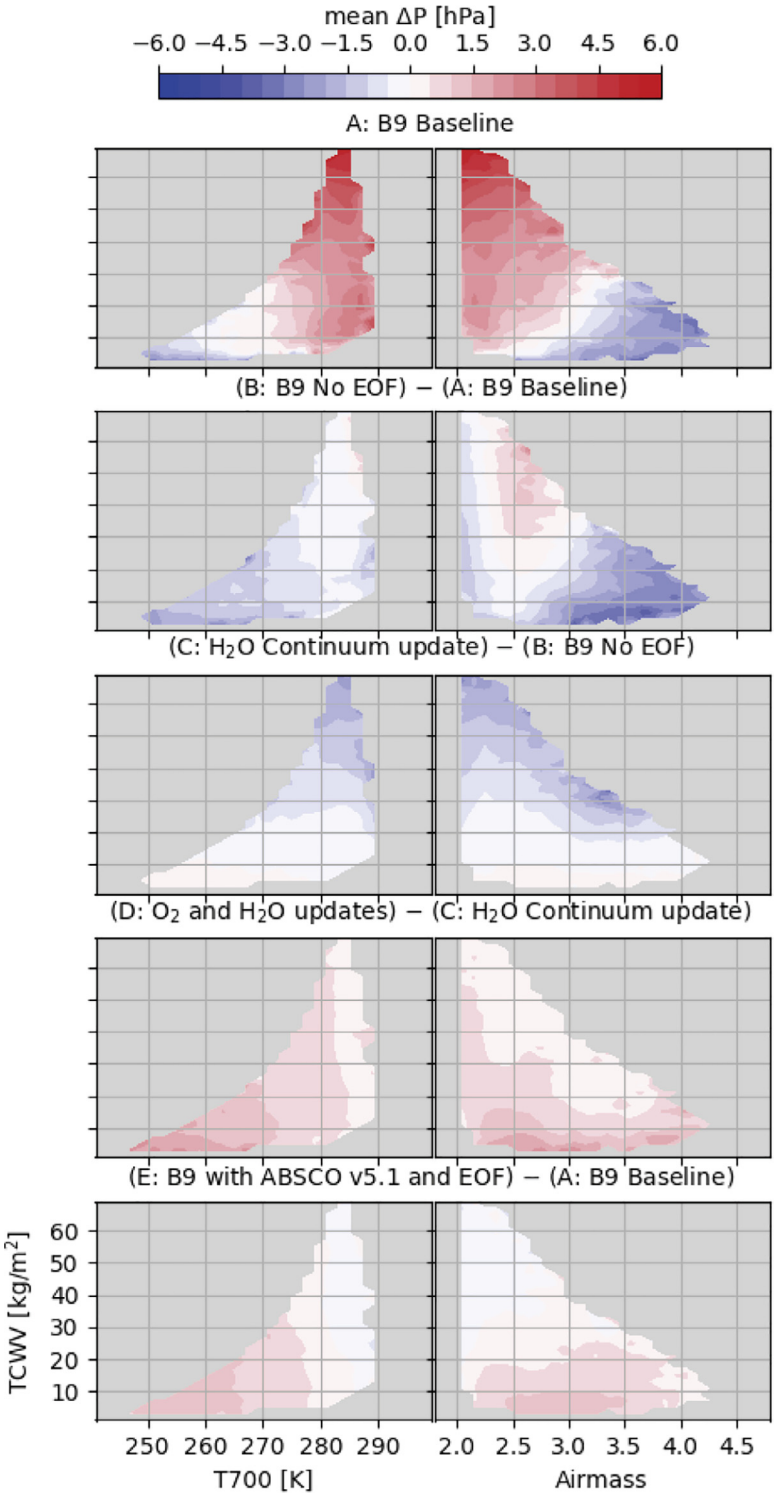

Fig. 11. Top row: Retrieved minus prior surface pressure (ΔP) for OCO-2 retrievals from the set of ocean glint soundings, as a function of 700 mbar temperature and total column water vapor (TCWV)(left column) and as a function of airmass and TCWV (right column) for the B9 baseline run (Test A, ABSCO v5.0 with corresponding EOFs). Subsequent rows show the impact of switching off the EOFs (Test B - Test A), the update to the H_2O continuum (Test C - Test B), the update to the O_2 spectroscopy (Test D - Test C) and finally the difference between Test E, which includes the updated H2O continuum and O2 spectroscopy (adopted for ABSCO v5.1) with re-calculated EOFs, and Test A (ABSCO v5.0 with EOFs). All plots use a common color bar (at top of figure), selected such that each contour is a step of 0.5 hPa in pressure.

veals smooth variation of the surface pressure bias with respect to temperature as shown in the upper left panel of Fig. 11. The surface pressure bias is negative (blue colors) for low temperatures, for larger H_2O column amounts. Also visible in this panel is a dependence of ΔP on H_2O column. The surface pressure bias is negative (blue colors) for low temperatures, and positive (red colors) for high temperatures. The region in which the surface pressure bias is negligible (less than 0.5 hPa in absolute value) is shown in white, and represents the observations within the 260–275 K range. The constant O_2 mixing ratio in the Earth's atmosphere indicates changes in O_2 spectroscopy would be expected to change the (color) gradient in the x-direction in both spaces, but

with potentially differing correlations for temperature and airmass with respect to the y-axis, column water vapor (CWV). Changes in H_2O spectroscopy would be expected to affect gradients in the y-direction, and the choices of temperature or airmass (for the x-axes) allow insight into desired separation of observational biases inherent in a solar reflectance measurement.

We found the subtle changes in ΔP (of -3 to +2 hPa) from our spectroscopic tests tend to be difficult to discern with a color scale that spans the total range of surface pressure biases. To better represent the changes associated with the L2 test set, we present the results as differences between the test results. The resulting $\delta\Delta P$ metric more directly reveals if one of the tests is an improvement relative to the previous test.

For example, in the second row of Fig. 11, comparing the $\delta\Delta P$ from the No-EOF test B versus the test A (the baseline): the patterns are similar, so it implies the negative bias in the baseline becomes increasingly negative (and vice versa). Thus the build 9 EOFs reduce absolute bias at the extremes of the climatology. However, there are also colored bins in the difference histogram in the unbiased area of the baseline test (between 260-275K), indicating that the EOFs are shifting the unbiased region. Another takeaway from the $\delta\Delta P$ plots with EOFs removed is the considerable amount of parameter space without absolute changes in ΔP less than 0.5 hPa in the histograms, indicating that the application of EOFs is only partially able to mitigate the biases in ΔP.

The third row of Fig. 11 indicates the effect of the H_2O continuum update (test C) in comparison to the no EOF baseline (test B). Here a decrease in ΔP is observed with higher water, and little effect is observed at low temperature/high air mass. This result is fully consistent with the strong temperature dependence of the H_2O partial pressure. The contour gradient is well matched to mitigate ΔP biases at high temperatures. The shapes of the contours in both climatological spaces are *inconsistent* with the EOF removal test, indicating that the EOFs were not compensating for this particular bias.

The O_2 spectroscopy update to the algorithm was tested in tandem with the H_2O continuum update, such that the difference plots on the fourth row of Fig. 11 are differences between tests D and C that focus on only the changes due to the O_2 spectroscopy update. The effects of this update are primarily positive shifts in the ΔP, and the pattern in the H_2O - temperature space is similar to the pattern observed (with opposite sign) with the EOF removed (second row of the figure). A comparison of these $\delta\Delta P$s in airmass space is not as directly correlated, with only the low H_2O portion tracking the anti-correlation.

In order to close the loop, EOFs were re-calculated using the same B9 L2 algorithm build, but with ABSCO v5.1 instead of ABSCO v5.0. The fifth row of Fig. 11 shows differences between tests E (B9 algorithm with ABSCO v5.1 and v5.1-based EOFs) and test A (B9 algorithm with ABSCO v5.0 and v5.0-based EOFs). These plots show that the overall impacts of the ABSCO update, after accounting for EOFs, are to (1) increase the mean surface pressure bias with respect to the prior, but (2) to reduce the dependence of the surface pressure bias on temperature, water vapor and airmass.

5. Discussion

In this section, we review the efforts described above and expand on items still awaiting further development.

H_2O continuum updates had non-negligible impact on satellite retrievals of surface pressure and XCO_2 in the tropics. The impact of the MT_CKD 3.2 update is mainly associated with changes to the dry-air continuum. Results of the tests with the ACOS/OCO algorithm point to the need for continued attention to laboratory and theoretical studies of the continuum.

Spectral residuals in the 1.6 µm and 2.06 µm CO_2 bands for both ground-based and satellite comparisons show evidence of outstanding systematic errors in H_2O lines, after retrieval of a scaling factor to a sonde-based (for ground-based measurements) or meteorological model (for spaceborne measurements) H_2O profiles. Total column H_2O values from OCO-2 have been shown to be a promising stand-alone product Nelson et al. [29]. Residuals well above the instrument noise were seen both for the HITRAN 2012 and HITRAN 2016 line lists. The choice of H_2O line list was shown to have a non-negligible impact on the retrieved XCO_2. It is possible that both the magnitude of the residuals and the impact on the retrieved XCO_2 could be mitigated by retrieving a H_2O profile, rather than a simple scaling of the initial guess. This is outside the scope of this work.

Nonetheless, the results of this work do point to the need for continued attention to H_2O line parameters both for the purposes of retrievals of well-mixed greenhouse gases and for H_2O retrievals from near-infrared radiances.

For O_2, the line mixing and CIA are intrinsically linked in the model adopted here. We define the CIA here according to the absorption that is not accounted for by the line contributions. Therefore, any changes to the modeling of the wings of the lines will also result in a change to the CIA. The CIA used in the ABSCO v5.1 tables was empirically determined using residual fits to ground-based atmospheric spectra. The bias in the retrieved surface pressure is sensitive to the details of the magnitude and shape of the O_2 CIA. We note that the CIA determined from the atmospheric measurements is not consistent with the CIA derived from residual fits to high pressure laboratory measurements. The O_2 updates presented here result in overall improvements in consistency between line shape/line mixing and CIA for ABSCO v5.1 relative to ABSCO v5.0. However, sawtooth features in spectral residuals, the shape of the leftover CIA from high-pressure lab measurements and the difference between shape of our atmospheric empirically-determined CIA and recent theoretical calculations from Karman et al. within the band all indicate that there is still definite scope for improvement in O_2 A-band spectroscopy, with the potential for further reduction in spectroscopy-related biases in remote sensing algorithms.

While the CO_2 spectroscopy was not updated between v5.0 and v5.1 of the OCO ABSCO tables, this does not mean that there is not also scope for improvement in the modeling of CO_2 absorption in the OCO bands. As discussed in Oyafuso et al. [33], there are outstanding issues with CO_2 spectroscopy in the OCO ABSCO tables that lead to systematic residuals above the level of the instrument noise. Hobbs et al. (2020) demonstrate that CO_2 spectroscopy uncertainties are expected to lead to region- and season-dependent biases in XCO_2 from the OCO algorithm. Updates to CO_2 spectroscopy will be a focus for future ABSCO table versions.

6. Conclusion

Development of high quality absorption coefficient tables that enable unbiased retrievals of surface pressure and XCO_2 has been a driving goal of the OCO missions. Improvements in physical parameterizations must be implemented and tested within a carefully developed, self consistent framework. The spectroscopy updates described in this manuscript result in an overall improvement in fits to atmospheric spectra and in a reduction in the spatial variability of the known surface pressure bias in OCO-2 B9 retrievals (with positive implications for a reduction in this term in the bias correction that is applied to the OCO XCO_2 products). The improvement is evident both with and without the use of EOFs in the algorithm. The ABSCO 5.1 tables have been implemented for the B10 Level 2 algorithm for OCO-2 and OCO-3. The tables are available on request from the authors, and will be made publicly

available with the B10 L2 data release. Despite the positive impact of the spectroscopic updates presented here, persistent systematic features remain in ground-based and satellite residuals with ABSCO v5.1. In future updates to the OCO ABSCO tables, we aim to implement further improvements to the O_2, CO_2 and H_2O spectroscopy.

Declaration of Competing Interest

The authors declare that they have no known competing financial interests or personal relationships that could have appeared to influence the work reported in this paper.

CRediT authorship contribution statement

Vivienne H. Payne: Supervision, Project administration, Methodology, Writing - original draft, Writing - review & editing. **Brian J. Drouin:** Conceptualization, Methodology, Investigation, Data curation, Software, Formal analysis, Writing - original draft, Writing - review & editing. **Fabiano Oyafuso:** Investigation, Software, Validation, Formal analysis, Data curation, Writing - original draft, Writing - review & editing. **Le Kuai:** Software, Formal analysis, Visualization, Writing - original draft, Writing - review & editing. **Brendan M. Fisher:** Software, Formal analysis, Writing - original draft, Writing - review & editing. **Keeyoon Sung:** Investigation, Formal analysis, Writing - original draft, Writing - review & editing. **Deacon Nemchick:** Investigation, Formal analysis, Writing - original draft, Writing - review & editing. **Timothy J. Crawford:** Investigation, Writing - original draft, Writing - review & editing. **Mike Smyth:** Software, Writing - original draft, Writing - review & editing. **David Crisp:** Supervision, Writing - original draft, Writing - review & editing. **Erin Adkins:** Investigation, Formal analysis, Writing - original draft, Writing - review & editing. **Joseph T. Hodges:** Supervision, Formal analysis, Writing - original draft, Writing - review & editing. **David A. Long:** Investigation, Formal analysis, Writing - original draft, Writing - review & editing. **Eli J. Mlawer:** Methodology, Formal analysis, Writing - original draft, Writing - review & editing. **Aronne Merrelli:** Formal analysis, Writing - original draft, Writing - review & editing. **Elizabeth Lunny:** Investigation, Writing - original draft, Writing - review & editing. **Christopher W. O'Dell:** Validation, Formal analysis, Writing - original draft, Writing - review & editing.

Acknowledgements

Portions of the research described in this paper was performed at the Jet Propulsion Laboratory, California Institute of Technology, under contract with NASA.

The authors gratefully acknowledge financial support from the U.S. Department of Energy, Office of Science, Office of Biological and Environmental Research, Environmental Sciences Division, as part of the ARM program under Grant DEFG02-90ER610. Support was also provided by the National Institute of Standards and Technology (NIST) Greenhouse Gas Measurements and Climate Research Program and the Orbiting Carbon Observatory (OCO) projects, National Aeronautics and Space Administration (NASA) Earth System Science Pathfinder (ESSP) missions. Manufacturers and product names are listed solely for completeness. These specific citations neither constitute an endorsement of the products nor imply that similar products from other companies would be less suitable. Copyright 2020 California Institute of Technology. Government sponsorship acknowledged.

Supplementary material

Supplementary material associated with this article can be found, in the online version, at 10.1016/j.jqsrt.2020.107217.

References

[1] Baker DF, Boesch H, Doney SC, O'Brien D, Schimel DS. Carbon source/sink information provided by column CO2 measurements from the orbiting carbon observatory. Atmos Chem Phys 2010;10(9):4145–65. doi:10.5194/acp-10-4145-2010.

[2] Baranov YI, Lafferty WJ. The water vapour self- and water-nitrogen continuum absorption in the 1000 and 2500 cm^{-1} atmospheric windows. Philos Trans R Soc A 2012;370(1968):2578–89. doi:10.1098/rsta.2011.0234.

[3] Benner DC, Devi VM, Sung K, Brown LR, Miller CE, Payne VH, et al. Line parameters including temperature dependences of air- and self-broadened line shapes of CO_2: 2.06-μm region. J Mol Spectrosc 2016;326:21–47. doi:10.1016/j.jms.2016.02.012.

[4] Campargue A, Kassi S, Mondelain D, Vasilchenko S, Romanini D. Accurate laboratory determination of the near-infrared water vapor self-continuum: a test of the MT_CKD model. J Geophys Res Atmos 2016;121(21):13180–203. doi:10.1002/2016JD025531.

[5] Chevallier F, Breon F-M, Rayner PJ. Contribution of the orbiting carbon observatory to the estimation of CO_2 sources and sinks: theoretical study in a variational data assimilation framework. J Geophys Res Atmos 2007;112(D9). doi:10.1029/2006JD007375.

[6] Cho C, Allin E, Welsh H. Effect of high pressures on infrared and red atmospheric absorption band systems of oxygen. Can J Phys 1963;41(12):1991–2002. doi:10.1139/p63-199.

[7] Connor B, Bösch H, McDuffie J, Taylor T, Fu D, Frankenberg C, et al. Quantification of uncertainties in OCO-2 measurements of XCO_2: simulations and linear error analysis. Atmos Meas Tech 2016;9:5227–38. doi:10.5194/amt-9-5227-2016.

[8] Crisp D, Pollock HR, Rosenberg R, Chapsky L, Lee RM, Oyafuso F, et al. The on-orbit performance of the orbiting carbon observatory-2 (OCO-2) instrument and its radiometrically calibrated products. Atmos Meas Tech 2017;10:59–81. doi:10.5194/amt-10-59-2017.

[9] Devi VM, Benner DC, Sung K, Brown LR, Crawford TJ, Miller CE, et al. Line parameters including temperature dependences of self- and air-broadened line shapes of CO_2: 1.6-μm region. J Quant. Spectrosc. RadiatTransf 2016;177(SI):117–44. doi:10.1016/j.jqsrt.2015.12.020.

[10] Drouin BJ, Payne V, Oyafuso F, Sung K, Mlawer E. Pressure broadening of oxygen by water. J Quant Spectrosc Radiat Transf 2014;133:190–8.

[11] Drouin BJ, Benner DC, Brown LR, Cich MJ, Crawford TJ, Devi VM, et al. Multispectrum analysis of the oxygen a-band. J Quant Spectrosc RadiatTransf 2017;186(SI):118–38. doi:10.1016/j.jqsrt.2016.03.037.

[12] Eldering A, Taylor TE, O'Dell CW, Pavlick R. The OCO-3 mission: measurement objectives and expected performance based on 1 year of simulated data. Atmos Meas Tech 2019;12(4):2341–70. doi:10.5194/amt-12-2341-2019.

[13] Fleisher AJ, Adkins EM, Reed ZD, Yi H, Long DA, Fleurbaey HM, et al. Twenty-five-fold reduction in measurement uncertainty for a molecular line intensity. Phys Rev Lett 2019;123(4). doi:10.1103/PhysRevLett.123.043001.

[14] Hartmann J-M, Tran H, Armante R, Boulet C, Campargue A, Forget F, et al. Recent advances in collisional effects on spectra of molecular gases and their practical consequences. J Quant Spectrosc RadiatTransf 2018;213:178–227. doi:10.1016/j.jqsrt.2018.03.016.

[15] Karman T, Koenis MAJ, Banerjee A, Parker DH, Gordon IE, van der Avoird A, et al. O_2-O_2 and O_2-N_2 collision-induced absorption mechanisms unravelled. Nat Chem 2018;10(5):549–54. doi:10.1038/s41557-018-0015-x.

[16] Karman T, Gordon IE, van der Avoird A, Baranov YI, Boulet C, Drouin BJ, et al. Update of the HITRAN collision-induced absorption section. ICARUS 2019;328:160–75. doi:10.1016/j.icarus.2019.02.034.

[17] Kiel M, O'Dell CW, Fisher B, Eldering A, Nassar R, MacDonald CG, et al. How bias correction goes wrong: measurement of XCO_2 affected by erroneous surface pressure estimates. Atmos Meas Tech 2019;12(4):2241–59. doi:10.5194/amt-12-2241-2019.

[18] Kulawik SS, Worden JR, McDuffie J, Wennberg P, Heald C, Wunch D, et al. Reducing regional biases from OCO-2 observations. San Francisco, CA: Fall Meeting of the American Geophysical Union; 2019.

[19] Kuze A, Suto H, Nakajima M, Hamazaki T. Thermal and near infrared sensor for carbon observation Fourier-transform spectrometer on the greenhouse gases observing satellite for greenhouse gases monitoring. Appl Opt 2009;48(35):6716–33. doi:10.1364/AO.48.006716.

[20] Levy A, Lacome N, Chackerian C. Collisional line mixing in spectroscopy of the Earth's atmosphere and interstellar medium.. Boston MA, 1992.: Academic Press; 1992.

[21] Long DA, Hodges JT. On spectroscopic models of the O_2 a-band and their impact upon atmospheric retrievals. J Geophys Res Atmos 2012;117. doi:10.1029/2012JD017807.

[22] Long DA, Havey DK, Okumura M, Miller CE, Hodges JT. O_2 a-band line parameters to support atmospheric remote sensing. J Quant Spectrosc RadiatTransf 2010;111(14):2021–36. doi:10.1016/j.jqsrt.2010.05.011.

[23] Long DA, Robichaud DJ, Hodges JT. Frequency-stabilized cavity ring-down spectroscopy measurements of line mixing and collision-induced absorption in the O_2 a-band. J Chem Phys 2012;137(1). doi:10.1063/1.4731290.

[24] McKellar A, Rich N, Welsh H. Collision-induced vibrational and electronic-spectra of gaseous oxygen at low-temperatures. Can J Phys 1972;50(1):1–9. doi:10.1139/p72-001.

[25] Miller CE, Crisp D, DeCola PL, Olsen SC, Randerson JT, Michalak AM, et al. Precision requirements for space-based X-CO2 data. J Geophys Res Atmos 2007;112(D10). doi:10.1029/2006JD007659.

[26] Mlawer E.J., D.G., Payne V.H.. Presentation given at the 2014 OCO-2 ABSCO meeting; 2014.
[27] Mlawer EJ, Payne VH, Moncet J-L, Delamere JS, Alvarado MJ, Tobin DC. Development and recent evaluation of the MT_CKD model of continuum absorption. Philos Trans R SocA 2012;370(1968):2520–56. doi:10.1098/rsta.2011.0295.
[28] Mondelain D, Manigand S, Kassi S, Campargue A. Temperature dependence of the water vapor self-continuum by cavity ring-down spectroscopy in the 1.6 μmtransparency window. J Geophys Res Atmos 2014;119(9):5625–39. doi:10.1002/2013JD021319.
[29] Nelson RN, Crisp D, Ott L, O'Dell C. W. High-accuracy measurements of total column water vapor from the Orbiting Carbon Observatory-2. Geophys Res Lett 2016;43 (12, 12,261–12,269). doi:10.1002/2016GL071200.
[30] O'Brien DM, Polonsky IN, Kumer JB. Sensitivity of remotely sensed trace gas concentrations to polarisation. Atmos Meas Tech 2015;8(11):4917–30. doi:10.5194/amt-8-4917-2015.
[31] O'Dell CW, Connor B, Boesch H, O'Brien D, Frankenberg C, Castano R, et al. The ACOS CO2 retrieval algorithm - part 1: description and validation against synthetic observations. Atmos Meas Tech 2012;5(1):99–121. doi:10.5194/amt-5-99-2012.
[32] O'Dell CW, Eldering A, Wennberg PO, Crisp D, Gunson MR, Fisher B, et al. Improved retrievals of carbon dioxide from Orbiting Carbon Observatory-2 with the version 8 ACOS algorithm. Atmos Meas Tech 2018;11(12):6539–76. doi:10.5194/amt-11-6539-2018.
[33] Oyafuso F, Payne VH, Drouin BJ, Devi VM, Benner DC, Sung K, et al. High accuracy absorption coefficients for the orbiting carbon observatory-2 (OCO-2) mission: validation of updated carbon dioxide cross-sections using atmospheric spectra. J Quant Spectrosc RadiatTransf 2017;203(SI):213–23. doi:10.1016/j.jqsrt.2017.06.012.
[34] Pieroni D, Nguyen-Van-Thanh, Brodbeck C, Claveau C, Valentin A, Hartmann J, et al. Experimental and theoretical study of line mixing in methane spectra. I. The N_2-broadened ν_3 band at room temperature. J Chem Phys 1999;110(16):7717–32. doi:10.1063/1.478724.
[35] Polonsky IN, O'Brien DM, Kumer JB, O'Dell CW, Team G. Performance of a geostationary mission, geoCARB, to measure CO_2, CH_4 and CO column-averaged concentrations. Atmos Meas Tech 2014;7(4):959–81. doi:10.5194/amt-7-959-2014.
[36] Richard L, Vasilchenko S, Mondelain D, Ventrillard I, Romanini D, Campargue A. Water vapor self-continuum absorption measurements in the 4.0 and 2.1 μm transparency windows. J Quant Spectrosc RadiatTransf 2017;201:171–9. doi:10.1016/j.jqsrt.2017.06.037.
[37] Robichaud DJ, Hodges JT, Brown LR, Lisak D, Maslowski P, Yeung LY, et al. Experimental intensity and lineshape parameters of the oxygen a-band using frequency-stabilized cavity ring-down spectroscopy. J Mol Spectrosc 2008;248(1):1–13. doi:10.1016/j.jms.2007.10.010.
[38] Rodgers CD. Inverse methods for atmospheric sounding - theory and practice, vol. 2. World Scientific Press; 2000. doi:10.1142/9789812813718.
[39] Rothman LS, Gordon IE, Babikov Y, Barbe A, Benner DC, Bernath PF, et al. The HITRAN2012 molecular spectroscopic database. J Quant Spectrosc RadiatTransf 2013;130(SI):4–50. doi:10.1016/j.jqsrt.2013.07.002.
[40] Smith K, Newnham D. Near-infrared absorption spectroscopy of oxygen and nitrogen gas mixtures. Chem Phys Lett 1999;308(1–2):1–6. doi:10.1016/S0009-2614(99)00584-9.
[41] Smith K, Newnham D. Near-infrared absorption cross sections and integrated absorption intensities of molecular oxygen (O_2, O_2-O_2, and O_2-N_2). J Geophys Res Atmos 2000;105(D6):7383–96. doi:10.1029/1999JD901171.
[42] Spiering FR, Kiseleva MB, Filippov NN, Naus H, van Lieshout B, Weijenborg C, et al. Line mixing and collision induced absorption in the oxygen a-band using cavity ring-down spectroscopy. The J Chem Phys 2010;133(11):114305.
[43] Spiering FR, Kiseleva MB, Filippov NN, van Lieshout B, van der Veen AMH, van der Zande WJ. The effect of collisions with nitrogen on absorption by oxygen in the a-band using cavity ring-down spectroscopy. Mol Phys 2011;109(4):535–42. doi:10.1080/00268976.2010.533709.
[44] Sung K, Toth RA, Brown LR, Crawford TJ. Line strength measurements of carbonyl sulfide ((OCS)-O-16-C-12-S-32) in the 2 nu(3), nu(1)+2 nu(2)+nu(3), and 4 nu(2)+nu(3) bands. J Quant Spectrosc RadiatTransf 2009;110(18):2082–101. doi:10.1016/j.jqsrt.2009.05.013.
[45] Sung K, Wishnow EH, Crawford TJ, Nemchick D, Drouin BJ, Toon GC, et al. FTS measurements of O_2 collision-induced absorption in the 565–700 nm region using a high pressure gas absorption cell. J Quant Spectrosc RadiatTransf 2019;235:232–43. doi:10.1016/j.jqsrt.2019.06.016.
[46] Tabisz G, Allin E, Welsh H. Interpretation of visible and near-infrared absorption spectra of compressed oxygen as collision-induced electronic transitions. Can J Phys 1969;47(24):2859–71. doi:10.1139/p69-349.
[47] Thompson DR, Chris Benner D, Brown LR, Crisp D, Malathy Devi V, Jiang Y, et al. Atmospheric validation of high accuracy CO_2absorption coefficients for the OCO-2 mission. J Quant Spectrosc Radiat Transf 2012;113(17):2265–76. doi:10.1016/j.jqsrt.2012.05.021.
[48] Toon G.C.. Personal Communication; 2019.
[49] Tran H, Hartmann JM. An improved O_2a band absorption model and its consequences for retrievals of photon paths and surface pressures. J Geophys Res Atmos 2008;113(D18). doi:10.1029/2008JD010011.
[50] Tran H, Boulet C, Hartmann JM. Line mixing and collision-induced absorption by oxygen in the a-band: laboratory measurements, model, and tools for atmospheric spectra computations. J Geophys Res D 2006;111(D15). doi:10.1029/2005jd006869.
[51] Turner DD, Clough SA, Lijegren JC, Clothiaux EE, Cady-Pereira KE, Gaustad KL. Retrieving liquid water path and precipitable water vapor from the atmospheric radiation measurement (ARM) microwave radiometers. IEEE Trans Geosci Remote Sens 2007;45(11):3680–90. doi:10.1109/tgrs.2007.903703.
[52] Ventrillard I, Romanini D, Mondelain D, Campargue A. Accurate measurements and temperature dependence of the water vapor self-continuum absorption in the 2.1 μm atmospheric window. J Chem Phys 2015;143(13). doi:10.1063/1.4931811.
[53] Wunch D, Toon GC, Wennberg PO, Wofsy SC, Stephens BB, Fischer ML, et al. Calibration of the total carbon column observing network using aircraft profile data. Atmos Meas Tech 2010;3(5):1351–62.
[54] Zhang LL, Yue TX, Wilson JP, Wang DY, Zhao N, Liu Y, et al. Modelling of XCO_2surfaces based on flight tests of tansat instruments. Sensors 2016;16(11). doi:10.3390/s16111818.